

1 Ancestry-dependent Enrichment of Deleterious Homozygotes in Runs of 2 Homozygosity

3
4 *Zachary A. Szpiech^{1,*}, Angel C.Y. Mak², Marquitta J. White², Donglei Hu², Celeste Eng², Esteban G.
5 Burchard², Ryan D. Hernandez^{1,3,4,5,6*}*

6
7 ¹ Department of Bioengineering and Therapeutic Sciences, University of California San Francisco, San
8 Francisco, California, USA.

9 ² Department of Medicine, University of California San Francisco, San Francisco, California, USA.

10 ³ Institute for Human Genetics, University of California San Francisco, San Francisco, California, USA.

11 ⁴ Quantitative Biosciences Institute, University of California San Francisco, San Francisco, California, USA.

12 ⁵ Department of Human Genetics, McGill University, Montreal, Quebec, Canada.

13 ⁶ Genome Quebec Innovation Center, McGill University, Montreal, Quebec, Canada.

14
15 * Corresponding authors: zachary.szpiech@ucsf.edu, ryan.hernandez@me.com

16 17 18 **Abstract**

19 Runs of homozygosity (ROH) are important genomic features that manifest when an
20 individual inherits two haplotypes that are identical-by-descent. Their length distributions are
21 informative about population history, and their genomic locations are useful for mapping recessive
22 loci contributing to both Mendelian and complex disease risk. We have previously shown that
23 ROH, and especially long ROH that are likely the result of recent parental relatedness, are
24 enriched for homozygous deleterious coding variation in a worldwide sample of outbred
25 individuals. However, the distribution of ROH in admixed populations and their relationship to
26 deleterious homozygous genotypes is understudied. Here we analyze whole genome sequencing
27 data from 1,441 individuals from self-identified African American, Puerto Rican, and Mexican
28 American populations. These populations are three-way admixed between European, African, and
29 Native American ancestries and provide an opportunity to study the distribution of deleterious
30 alleles partitioned by local ancestry and ROH. We re-capitulate previous findings that long ROH
31 are enriched for deleterious variation genome-wide. We then partition by local ancestry and show
32 that deleterious homozygotes arise at a higher rate when ROH overlap African ancestry segments
33 than when they overlap European or Native American ancestry segments of the genome. These
34 results suggest that, while ROH on any haplotype background are associated with an inflation of

35 deleterious homozygous variation, African haplotype backgrounds may play a particularly
36 important role in the genetic architecture of complex diseases for admixed individuals, highlighting
37 the need for further study of these populations.

38 **Introduction**

39 Runs of Homozygosity (ROH) are long stretches of identical-by-descent (IBD) haplotypes
40 that manifest in individual genomes as the result of recent parental relatedness. Originally
41 conceived to improve the accuracy of homozygosity mapping of recessive Mendelian diseases,
42 ROH have formed the foundation of studies investigating the contribution of recessive deleterious
43 variants to the genetic risk for complex diseases and the to the determination of complex traits [1].
44 Moreover, they have provided unique insights into the demographic and sociocultural processes
45 [1] that have shaped genomic variation patterns in contemporary worldwide human populations [2-
46 12], ancient hominins [13-16], non-human primates [17, 18], woolly mammoths [19], livestock [20-
47 26], birds [27, 28], felines [29], and canids [30-39]. Recent population bottlenecks, cultural
48 preferences for endogamy or consanguineous marriage, and natural selection, can create
49 increased rates of ROH in individual genomes, substantially increasing overall homozygosity in
50 such populations.

51 Several studies of the distribution of ROH in ostensibly outbred human populations have
52 shown that ROH are common and range in size from tens of kilobases to several megabases in
53 length [2-8]. Furthermore, total length and prevalence of ROH are correlated with distance from
54 Africa [5, 7, 8], with more and longer ROH manifesting in individuals from populations a longer
55 distance away. These patterns likely reflect increased IBD among haplotypes as a result of the
56 serial bottleneck process that humans experienced as they migrated out of Africa.

57 The prevalence of ROH in individual genomes has also been an important factor for
58 understanding the genetic basis of complex phenotypes [40-43]. High levels of ROH have been
59 associated with heart disease [44-47], cancer [44, 48-52], blood pressure [53-57], LDL cholesterol

60 [57], various mental disorders [58-63], human height [64, 65], and increased susceptibility to
61 infectious diseases [66]. Indeed, these results are consistent with the idea that many rare alleles
62 of small effect may be the cause of increased risk for complex diseases [67-71], especially if these
63 mutations are recessive [4, 72].

64 We have previously shown that ROH, especially long ROH, are enriched for deleterious
65 homozygous variation [73, 74]. Whereas an overall increase in homozygotes is expected with
66 increasing genomic ROH, we have shown that the rate at which deleterious homozygotes
67 accumulate outpaces the rate at which benign homozygotes accumulate [73, 74] in long ROH
68 (ROH on the order of several megabases). This result is a consequence of young (long)
69 haplotypes with low-frequency variants segregating on them being paired IBD [74]. As low-
70 frequency variants are more likely to be deleterious, the processes that create very long ROH can
71 also generate unusually high numbers of deleterious homozygotes within these regions.

72 Although a few studies describing the worldwide distribution of ROH patterns have included
73 a small number of admixed populations [5, 7, 8], the number of individuals per admixed population
74 has been fairly small. Even as the number of admixed individuals continues to grow in the United
75 States [75], they are still relatively understudied, which translates to disparities in our
76 understanding of population-specific genetic factors that may influence complex phenotypes [76,
77 77]. Indeed, admixed populations have unique features compared to other populations, in that
78 genomes from these populations are recent combinations of two or more ancestral populations.

79 This ancestral mosaicism has been exploited to make inferences about the natural history
80 of human populations [78-88] and to search for ancestral haplotypes that influence complex
81 phenotypes [89-96]. Here we add to the body of work on admixed populations by examining the
82 relationship between ROH, local ancestry, and the accumulation of deleterious alleles. We use
83 1,441 recently published [97] whole genome sequences (dbGaP accession numbers phs000920
84 and phs000921) distributed roughly equally across three admixed populations in the Americas:

85 African American ($n = 475$), Mexican American ($n = 483$), and Puerto Rican ($n = 483$). Each of
86 these populations is three-way admixed between European, Native American, and African
87 ancestral populations, although each has a distinct history.

88 Among the ancestral populations that contributed haplotypes to these admixed populations,
89 it has been shown that the distribution of deleterious heterozygotes and deleterious homozygotes
90 changes with distance from Africa [98-101]. With this in mind, we propose that accumulation of
91 deleterious homozygotes via increased genomic ROH may also differ within admixed populations
92 based on differing ancestral haplotypes. Indeed, with high deleterious heterozygosity, we propose
93 that African ancestral haplotypes may be most susceptible to large increases in deleterious
94 homozygotes when subjected to harsh bottlenecks or inbreeding, as these low frequency
95 deleterious alleles will be paired into homozygotes as a result of increased genomic ROH.

96

97 **Results**

98 **Admixture**

99 Using the subset of sites from our whole-genome sequencing data that intersected with our
100 African, European, and Native American reference panels, we called 3-way local ancestry tracts in
101 all 1,441 samples (see Methods). We also estimated global ancestry proportions by summing the
102 length of all haplotypes inferred to be from a given ancestry and dividing by the total genome
103 length. Fig 1 summarizes the global ancestry proportions for all individuals from each population
104 on a ternary plot. The admixture proportions largely accord with previous results in these
105 populations, with Puerto Ricans having mostly African and European ancestry, Mexican
106 Americans having mostly European and Native American ancestry, and African Americans having
107 mostly African and European ancestry to the near exclusion of any Native American ancestry.
108 However, although African Americans are frequently treated as a 2-way admixed population
109 between European and African sources, we show that several AA individuals have non-trivial

110 proportions of Native American ancestry. This suggests that, in general, a 2-way admixture model
111 may not be uniformly appropriate for studying admixture patterns amongst self-identified African
112 American individuals.

113 **Runs of Homozygosity**

114 We followed the ROH calling pipeline of Pemberton et al. [7] as implemented in the
115 software GARLIC [102] to call ROH from the full whole-genome sequencing data (see Methods).
116 This method identifies three classes of ROH based on the length distribution in each population.
117 We refer to these size classes as short, medium, and long. These classes roughly correspond to
118 ROH formed of IBD haplotypes from different time periods from the population history. Short ROH
119 are tens of kilobases in length and likely reflect the homozygosity of old haplotypes; medium ROH
120 are hundreds of kilobases in length and likely reflect background relatedness in the population;
121 and long ROH are hundreds of kilobases to several megabases in length and are likely the result
122 of recent parental relatedness. Total length of ROH in the genome is correlated with distance
123 from Africa [4, 7]. In the case of our admixed populations, we therefore expect the total length of
124 ROH to be correlated with increased European and Native American admixture fraction. Indeed,
125 Fig 2A illustrates this pattern, with AA individuals having lowest total ROH, PR individuals having
126 intermediate total ROH, and MX individuals having the highest total ROH (all pairwise Mann-
127 Whitney U tests $p < 2.2 \times 10^{-16}$). Breaking down ROH by size class, we find that the total length
128 of short ROH is comparable between PR and MX individuals (Fig 2B), but the total length of both
129 medium ROH (Fig 2C) and total long ROH (Fig 2D) is highest on average in MX individuals.

130 **Deleterious Alleles**

131 We used multiple approaches to predict the deleteriousness of all sites in the genome (see
132 Methods), but focus on missense mutations classified as Probably Damaging, Possibly Damaging,
133 or Benign using Polyphen 2 [103]. As in [73], we combine the Probably Damaging and Possibly
134 Damaging mutations into a single “damaging” class, and we combine all Benign mutations with

135 synonymous mutations into a single “benign” class. For individual i across all sites, we denote by
136 $g_i^{d,k}$ and $g_i^{b,k}$ the total number of sites with $k \in \{0,1,2\}$ alternate alleles classified as damaging or
137 benign, respectively. In Fig 3A we plot the distribution of deleterious heterozygotes per individual,
138 $g_i^{d,1}$, split by population. Consistent with previous work [98-101], we see an increased number of
139 deleterious heterozygotes in populations with more African ancestry, with AA individuals having
140 the most and MX individuals having the fewest (patterns replicate with other deleterious
141 categories, see S5-S10 Figs). Conversely, we would expect an increase of deleterious
142 homozygotes per individual in populations with more non-African ancestry. Indeed, in Fig 3B we
143 plot the distribution of deleterious homozygotes per individual, $g_i^{d,2}$, split by population and
144 observe AA individuals with the fewest and MX individuals having the most (these patterns also
145 replicate with other deleterious categories, see S5-S10 Figs). Figure 3C plots the total number of
146 deleterious alleles per individual ($g_i^{d,1} + 2g_i^{d,2}$). Contrary to other work [101], we find a total
147 deleterious load highest on average in AA individuals. Although this pattern replicates across
148 several other deleterious calling methods (S5-S9 Figs), when using GERP scores (as in [101]) the
149 pattern reverses (S10 Fig) and is consistent with [101].

150 **Deleterious Alleles Across Local Ancestry**

151 We next investigate whether there are any differences in deleterious load by local ancestry.
152 Although our local ancestry calls provide us with phased local ancestry inferences, we were
153 limited to a small subset of sites for our reference populations. Since the vast majority of our
154 deleterious alleles come from our unphased whole-genome data, we do not have phase
155 information for the deleterious alleles and cannot assign a specific ancestral haplotype in regions
156 of discordant ancestry. Therefore, we calculate total load based on six different ancestry
157 backgrounds. AFR, EUR, and NAM ancestry regions represent regions that are homozygous for
158 African, European, and Native American ancestries, respectively, and AFEU, EUNA, and AFNA
159 ancestry regions represent regions that are called heterozygous for African/European,

160 European/Native American, and African/Native American ancestries, respectively. We then
161 calculate for each population the number of deleterious alleles per basepair for each ancestry
162 background.

163 Table 1 shows the number of deleterious alleles per basepair for each population and each
164 ancestry background. We perform two types of tests for independence in order to determine
165 whether there are significant differences in the number of deleterious alleles per basepair. First,
166 we test for independence of the count of deleterious alleles on an ancestry background and the
167 count of basepairs covered by that ancestry across populations. We find that neither African
168 ancestry nor European ancestry have statistical differences in the number of deleterious alleles
169 per MB across populations. Further, while NAM, EUAF, and AFNA exhibit statistically differences
170 across populations, it appears to be driven by one of the two populations (AA, MX, and PR,
171 respectively). Next, we test for independence of these counts across ancestries within each
172 population. Here we find that all populations have statistically significant differences in the
173 distribution of deleterious alleles across ancestry backgrounds (AA $p < 2.2 \times 10^{-16}$; MX $p < 2.2 \times$
174 10^{-16} ; PR $p < 2.2 \times 10^{-16}$), with NAM ancestry having the lowest rate in AA and PR individuals
175 and EUR having the lowest rate in MX individuals. However, we note that the overall differences
176 were very small (a difference of < 0.1 deleterious alleles per Mbp).

177 **Deleterious Alleles in ROH**

178 Next, we turn to examining the distribution of deleterious homozygotes within ROH. It was
179 previously reported [73, 74] that there is a higher proportion of deleterious homozygotes per unit
180 increase of ROH than expected from the proportion of benign homozygotes. Naturally, as the
181 total amount of genomic ROH increases, we expect more homozygotes to fall within ROH.
182 However, [73] and [74] found that the rate of increase of the proportion of deleterious
183 homozygotes was greater than for benign homozygotes. This effect was strongest for long ROH,
184 which are likely the result of recent parental relatedness.

185 For each individual i and for each ROH class $j \in \{A, B, C, R, N\}$ (A - short ROH, B - medium
186 ROH, C - long ROH, R - all ROH, and N - outside ROH), we define the number of damaging or
187 benign sites with $k \in \{0, 1, 2\}$ alternate alleles as $g_{i,j}^{d,k}$ and $g_{i,j}^{b,k}$, respectively. Thus we calculate the
188 proportion of damaging homozygotes in ROH class j as

$$f_{i,j}^d = \frac{g_{i,j}^{d,2}}{g_{i,R}^{d,2} + g_{i,N}^{d,2}}$$

189 and the proportion of benign homozygotes in ROH as

$$f_{i,j}^b = \frac{g_{i,j}^{b,2}}{g_{i,R}^{b,2} + g_{i,N}^{b,2}}$$

190 respectively. We also compute, for each individual i and each class j , the fraction of the genome
191 covered in ROH as

$$G_{i,j} = \frac{\text{total length of ROH regions of class } j \text{ in individual } i}{\text{total genome length}}$$

192 We plot the proportions of ROH homozygotes versus genomic fraction of ROH in Fig 4,
193 which is analogous to Fig 4 from [73]. In order to determine if there is a statistically significant
194 difference in the accumulation of deleterious homozygotes versus benign homozygotes, we
195 construct a linear regression model (as in [73, 74]), $f_{\cdot,j} = \beta_0 + \beta_1 G_{\cdot,j} + \beta_2 D + \beta_3 D G_{\cdot,j} + \varepsilon$, where $f_{\cdot,j}$
196 is a vector of length 2,882 containing the proportions of both damaging and benign homozygotes
197 in ROH class j for all individuals, $G_{\cdot,j}$ is a vector of genomic class j ROH proportions, and D is an
198 indicator variable taking a value of 1 when the response represents damaging homozygotes and 0
199 for benign homozygotes. In this framework, a statistically significant β_2 suggests an overall higher
200 proportion of damaging homozygotes in ROH compared to benign homozygotes, e.g. $\beta_2 = 0.1$
201 means that an extra 10% of genome-wide deleterious homozygotes fall in ROH compared to the
202 distribution of benign homozygotes. A statistically significant β_3 suggests a difference in the rate of
203 accumulation per unit increase of ROH, e.g. $\beta_3 = 1.0$ means that for a 10% increase in genomic

204 ROH, 10% more deleterious homozygotes fall in ROH compared to benign homozygotes. Inferred
205 coefficients for the four regressions corresponding to each $j \in \{A, B, C, R\}$ are given in Table 2.

206 Fig 4A plots these proportions versus total ROH for all ROH classes combined. In
207 agreement with [73], we find that there is an overall greater proportion of damaging homozygotes
208 in ROH compared to benign homozygotes ($\beta_2 = 0.1799$, $p < 2 \times 10^{-16}$), but in contrast the
209 overall rate of accumulation is not different ($\beta_3 = 1.807 \times 10^{-2}$, $p = 0.0671$). When we partition
210 ROH by size class, the distribution of homozygotes in short ROH (Fig 4B) also differs from [73].
211 Whereas previously there were no statistically significant differences in β_2 or β_3 , here we find a
212 significant positive $\beta_2 = 4.810 \times 10^{-2}$ ($p < 2 \times 10^{-16}$) and a statistically significant negative
213 $\beta_3 = -0.428$ ($p = 1.10 \times 10^{-8}$) suggesting that ROH comprised of old haplotypes accumulate
214 deleterious homozygotes at a slower rate than benign homozygotes. As we expect short ROH to
215 be comprised of old haplotypes that have been segregating for a long time, it is reasonable to
216 think that only haplotypes with relatively few deleterious alleles remain segregating in the
217 population. Our results for medium (Fig 4C) and long ROH (Fig 4D) are consistent with previous
218 work [73, 74]; in particular we find that the difference in rates of gain of deleterious versus benign
219 homozygotes is greatest in long ROH ($\beta_3 = 0.229$; $p < 2 \times 10^{-16}$).

220 **Deleterious Alleles in ROH Partitioned by Local Ancestry**

221 Now we turn to analyzing the distribution of deleterious homozygotes in ROH comprised of
222 only one particular ancestral haplotypes. As shown in Fig 3A and in other work [98-101],
223 populations with more African ancestry tend to have high numbers of deleterious heterozygotes
224 genome-wide. This contrasts with populations that have more European and Native American
225 ancestry, which tend to have more genome-wide deleterious homozygotes (Fig 3B) as a result of
226 the serial bottlenecks they experienced since migrating out of Africa.

227 However, admixed populations are a recent combination of two or more ancestral
228 populations, and since genome-wide ancestry proportions correlate with numbers of deleterious

229 heterozygotes and homozygotes, we desire to investigate how this mosaicism might affect the
230 accumulation of deleterious homozygotes in ROH. We have already shown (Fig 4) that as total
231 genomic ROH increases the proportion of deleterious homozygotes falling in ROH increases
232 faster than the proportion of benign homozygotes, but here we want to know if the ancestral
233 background of the IBD haplotypes matters. Here we propose that haplotypes sourced from
234 ancestral populations with high deleterious heterozygosity have highest rates of accumulation of
235 deleterious homozygotes when paired IBD to generate ROH.

236 Why might we expect high deleterious heterozygosity haplotypes to generate large
237 numbers of deleterious homozygotes in ROH? Pemberton and Szpiech [74] recently
238 demonstrated that long ROH are enriched for homozygotes comprised of low-frequency alleles.
239 Low-frequency alleles are more likely to be deleterious and are more likely to manifest in
240 individual genomes as heterozygotes. Under a typical random mating scenario these low
241 frequency alleles would be likely to segregate in the population largely as heterozygotes, however
242 severe bottlenecks and cultural practices such as endogamy and consanguineous marriage
243 substantially raise the likelihood of pairing low-frequency alleles as IBD homozygotes. We
244 therefore expect that deleterious homozygotes will be concentrated in large proportion within ROH
245 comprised of African ancestral haplotypes, and that the rate of gain of deleterious homozygotes
246 will be greatest in ROH of African ancestral haplotypes.

247 To test this proposition, we first partition ROH based on the ancestral background of the
248 underlying IBD haplotypes. Then we compute for each individual (i) the fraction of all deleterious
249 (d) and benign (b) homozygotes across the genome that fall into each ROH class (j) as:

$$f_{i,j}^d(A) = \frac{g_{i,j}^{d,2}(A)}{g_{i,R}^{d,2} + g_{i,N}^{d,2}}$$

250 and

$$f_{i,j}^b(A) = \frac{g_{i,j}^{b,2}(A)}{g_{i,R}^{b,2} + g_{i,N}^{b,2}}$$

251 where $g_{i,j}^{d,2}(A)$ and $g_{i,j}^{b,2}(A)$ are the number of deleterious and benign homozygotes, respectively,
252 in individual i in ROH class j on ancestral haplotype background $A \in \{AFR, EUR, NAM\}$. Similarly,
253 $f_{i,j}^d(A)$ and $f_{i,j}^b(A)$ are the genome-wide fraction of deleterious and benign homozygotes,
254 respectively, in individual i in ROH class j that fall on haplotype background A . Finally, we fit a
255 linear model similar as above, $f_{i,j}(A) = \beta_0 + \beta_1 G_{i,j}(A) + \beta_2 D + \beta_3 D G_{i,j}(A) + \varepsilon$, in order to test for
256 differences in the rate of accumulation (β_3) of deleterious homozygotes compared to benign
257 homozygotes as a function of $G_{i,j}(A)$, the genomic fraction of ROH on ancestral background A .
258 The results are plotted in Fig 5 for total ROH ($j = N$; Fig 5A-C) and for long ROH ($j = C$; Fig 5D-
259 F), and the regression coefficients are also summarized in Table 3.

260 For total ROH, we find significant differences in the rate of accumulation of deleterious
261 homozygotes on all ancestry backgrounds (Fig 5A-C). Furthermore, consistent with our
262 expectations, we find that ROH on African ancestral haplotypes have the highest rate difference
263 ($\beta_3 = 1.214, p < 2 \times 10^{-16}$; Fig 5C), whereas ROH on European ancestral haplotypes have an
264 intermediate rate difference ($\beta_3 = 0.648, p < 2 \times 10^{-16}$; Fig 5B) and ROH on Native American
265 ancestral haplotypes have the lowest rate difference ($\beta_3 = 0.510, p < 2 \times 10^{-16}$; Fig 5A). This
266 pattern is repeated when we consider only long ROH comprised of young haplotypes (Fig 5D-F)
267 and also when we analyze smaller ROH (albeit with weaker effects; S1 Fig).

268 We next directly compare the rate of increase of deleterious homozygotes across different
269 ancestral haplotype backgrounds. To do this we compute the following regression,
270 $f_{i,j}^d(\cdot) = \beta_0 + \beta_1 G_{i,j}(\cdot) + \beta_2 I(EUR) + \beta_3 I(NAM) + \beta_4 I(EUR)G_{i,j}(\cdot) + \beta_5 I(NAM)G_{i,j}(\cdot) + \varepsilon$, where
271 $f_{i,j}^d(\cdot)$ is a vector representing the proportion of damaging homozygotes in ROH class j on each
272 local ancestry background across all individuals. $G_{i,j}(\cdot)$ represents the genome-wide fraction ROH

273 class j falling on each local ancestry background across all individuals, and $I(A)$ is an indicator
274 variable which takes the value 1 if the associated response is on ancestral background $A \in$
275 $\{AFR, EUR, NAM\}$ and takes the value 0 otherwise. Here we analyze each ROH class: all, long,
276 medium, and short.

277 We plot the results for “all” and “long” in Fig 6 (“medium” and “short” in S2 Fig) and
278 summarize the inferred regression coefficients for all classes in Table 4. We focus on the
279 regression coefficients β_4 and β_5 , which represent the difference in rate of gain of deleterious
280 homozygotes in ROH on European or Native American haplotypes compared to African
281 haplotypes, respectively. Graphically, in Fig 6 and S2 Fig, a significant β_4 corresponds to a
282 significant difference in the slope of the orange and blue line, and a significant β_5 corresponds to a
283 significant difference in the slope of the orange and purple line. Since we expect that the rate of
284 gain of deleterious homozygotes to be lowest in ROH on European and Native American
285 haplotypes compared to ROH on African ones, we expect significant negative values for both β_4
286 and β_5 .

287 Consistent with our expectations, when analyzing all ROH (Fig 6A) we find a significant
288 negative $\beta_4 = -0.763$ ($p < 2 \times 10^{-16}$) and $\beta_5 = -0.852$ ($p < 2 \times 10^{-16}$), indicating that the gain
289 rate of damaging homozygotes in ROH on African ancestral haplotypes outpaces that of ROH on
290 the other ancestral haplotypes. This pattern continues when considering only long ROH ($\beta_4 =$
291 -0.852 , $p < 2 \times 10^{-16}$; $\beta_5 = -0.727$, $p < 2 \times 10^{-16}$; Fig 6B) and smaller ROH (Table 4 and S2
292 Fig).

293 To check the robustness of these results, we reran these analyses using several other
294 deleterious classification methods including SIFT [104, 105], Provean [106], and GERP [107].
295 Since GERP scores sites and not mutations, we restricted the GERP analysis to loci where the
296 ancestral and derived states were inferred to high confidence. As this ancestral polarization
297 results in discarding a large number of loci with ambiguous ancestral allele state, we also reran

298 these analyses for Polyphen 2 [103], SIFT [104, 105], and Provean [106] restricted only to loci for
299 which we have ancestral/derived state information. S3 Fig plots the inferred β_3 for each of these
300 analyses for each ROH size class and demonstrates qualitatively similar patterns as shown
301 above.

302 We further re-analyzed a subset of the ROH and deleteriousness calls from Pemberton and
303 Szpiech [74], which contains data on six admixed populations from the 1000 Genomes Project
304 [108] and used CADD [109] scores as a deleteriousness prediction (S1 Text). After extracting the
305 data relating to the admixed individuals from Pemberton and Szpiech [74] and calling local
306 ancestries, we again find qualitatively similar patterns as above (S4 Fig).

307 Finally, since Pemberton and Szpiech [74] showed that these enrichment patterns appear
308 to be driven by an abundance of homozygotes in ROH comprised of low-frequency alleles, we re-
309 analyzed our data using categories of minor allele frequency (MAF) instead of deleteriousness. In
310 order to determine MAF category, we use frequencies computed from all TOPMed Freeze 3
311 whole-genome sequencing data sets (dbGaP accession numbers phs000920, phs000921,
312 phs001062, phs001032, phs000997, phs000993, phs001189, phs001211, phs001040,
313 phs001024, phs000974, phs000956, phs000951, phs000946, phs000988, phs000964,
314 phs000972, phs000954, and phs001143) forming a total sample size of $n = 18,581$. Using these
315 allele frequencies, we categorize each polymorphic locus in a gene region (exons plus introns)
316 into one of two categories: common ($MAF \geq 0.05$) and rare ($MAF < 0.05$). We then fit the same
317 models as above, except that instead of comparing the proportion of deleterious alternate allele
318 homozygotes to benign homozygotes as a function of ROH coverage, we compare the number of
319 minor allele homozygotes in the rare class to the common class.

320 We summarize the results of these analyses for each ancestral background, each ROH
321 size class, and each low-frequency class in Fig 7. We find that ROH on African haplotype
322 backgrounds are gain more low-frequency minor allele homozygotes per unit increase of ROH

323 (and especially long class C ROH) compared to common minor allele homozygotes. Since low
324 frequency alleles are enriched for deleterious variants relative to high frequency alleles, this result
325 accords with our previous analyses.

326

327 **Discussion**

328 The distribution of runs of homozygosity in individual genomes has provided insights into
329 evolutionary, population, and medical genetics [1]. By examining their genomic location and
330 prevalence in a population, we can learn about the history and adaptation of natural populations
331 [2-39], and we can make discoveries about the genetic basis of complex phenotypes [40-66].
332 Given the importance of demographic history and socio-cultural practices in the generation of
333 ROH in individual genomes, and their relationship to complex phenotypes including many genetic
334 diseases, it naturally follows to study the distribution of deleterious alleles and their relationship to
335 ROH.

336 Previous work has described the effect of demographic history on the distribution of
337 deleterious alleles [98-101, 110, 111], including a few specifically investigating their relationship
338 with runs of homozygosity [21, 38, 73, 74, 112, 113]. However, little work has been done on the
339 relationship between deleterious alleles and ROH in admixed populations (although see [113]).
340 Since there is evidence of very recent bottlenecks (which generate ROH) within admixed
341 populations living in the Americas [88, 113], the relationship between ROH and the accumulation
342 of deleterious homozygotes may provide valuable insights into the genetic basis of complex
343 phenotypes in these individuals.

344 Here we analyzed 1,441 individuals across three admixed populations: African American,
345 Puerto Rican, and Mexican American. We found that, consistent with other studies, the proportion
346 of deleterious homozygotes found in ROH increases faster than the proportion of benign
347 homozygotes as a function of total genomic ROH (Fig 4). However, we also proposed that

348 ancestral haplotypes from populations with high deleterious *heterozygosity* would exhibit even
349 greater increases of deleterious homozygotes per unit ROH. We reason that, under random
350 mating, the larger number of low-frequency deleterious alleles in the population would largely
351 segregate as heterozygotes, whereas, when a harsh bottleneck or consanguinity occurs, these
352 mutations get paired IBD as homozygotes, concentrating more deleterious homozygotes within
353 ROH. Indeed, we found that the genome-wide proportion of deleterious homozygotes in ROH on
354 African ancestral haplotypes increased faster per unit ROH than on either European or Native
355 American ancestral haplotypes (Figs 5 and 6). These patterns are also consistent with population-
356 specific worldwide patterns of deleterious homozygotes in ROH [74], where three of the five
357 African populations analyzed had among the highest rates of enrichment in long ROH.

358 Whereas ROH on any haplotype background are associated with an increased rate of
359 deleterious homozygotes, ROH on African haplotypes tend to have a larger share of the genome-
360 wide deleterious homozygotes. Indeed, this accords with recent work that has independently
361 associated increased ROH [65] and increased African ancestry [114] with reduced lung function.
362 This suggests that these ROH on African haplotypes may play a particularly important role in the
363 genetic architecture of complex phenotypes in admixed individuals, especially for populations with
364 African ancestry that have undergone very harsh bottlenecks in the recent past.

365

366 **Methods**

367 **Calling Local Ancestry**

368 We used 90 African (YRI) individuals and 90 European (CEU) individuals for ancestry
369 references (genotypes obtained from the Axiom[®] Genotype Data Set at
370 [https://www.thermofisher.com/us/en/home/life-science/microarray-analysis/microarray-data-](https://www.thermofisher.com/us/en/home/life-science/microarray-analysis/microarray-data-analysis/microarray-analysis-sample-data/axiom-genotype-data-set.html)
371 [analysis/microarray-analysis-sample-data/axiom-genotype-data-set.html](https://www.thermofisher.com/us/en/home/life-science/microarray-analysis/microarray-analysis-sample-data/axiom-genotype-data-set.html)) and SNPs with less than

372 95% call rate were removed. For Native American reference genotypes we used 71 Native
373 American individuals previously genotyped on the Axiom[®] Genome-Wide LAT 1 array [115].

374 We then subset our 1,441 whole-genome sequences corresponding to sites found on the
375 Axiom[®] Genome-Wide LAT 1 array, leaving 765,321 markers. We then merge these data with our
376 European (CEU), African (YRI), and Native American (NAM) reference panels, which overlapped
377 at 434,145 markers. After filtering multi-allelic SNPs and SNPs with > 10% missing data, we
378 obtained a final merged dataset of 428,644 markers. We phased this combined data set using
379 SHAPEIT2 [116] and called local ancestry tracts jointly with RFMix [117] under a three-way
380 admixture model based on the African, European, and Native American reference genotypes
381 described above.

382 **Calling Runs of Homozygosity**

383 We called runs of homozygosity using the program GARLIC v1.1.4 [102], which implements
384 the ROH calling pipeline of [7], for each population separately on the full whole-genome call set,
385 filtering only monomorphic sites. For the 475 African American (AA) individuals, this left
386 39,517,679 segregating sites; for the 483 Puerto Rican (PR) individuals, this left 31,961,900
387 segregating sites; and for the 483 Mexican American (MX) individuals, this left 30,744,389
388 segregating sites. Instead of asserting a single constant genotyping error rate (as in [7]), we used
389 genotype quality scores provided with the WGS data to give GARLIC a per-genotype estimation of
390 error. Using GARLIC's rule of thumb parameter estimation, we chose analysis window sizes of
391 290 SNPs, 250 SNPs, and 210 SNPs for the AA, PR, and MX populations, respectively. Using
392 GARLIC's rule of thumb parameter estimation, we chose overlap fractions of 0.3688, 0.3553, and
393 0.3528 for the AA, PR, and MX populations, respectively. GARLIC chose LOD score cutoffs of -
394 47.5169, -70.1977, and -60.9221 for the AA, PR, and MX populations, respectively. Using a
395 three-component Gaussian mixture model, GARLIC determined class A/B and class B/C size

396 boundaries as 38,389 bps and 142,925 bps for AA; as 50,618 bps and 230,079 bps for PR; and
397 46,979 bps and 217,054 bps for MX.

398 **Calling Deleterious Alleles**

399 Using the Whole Genome Sequencing Annotation (WGSA) pipeline [118] to generate
400 annotation data, we extracted PolyPhen 2 [103], SIFT [104, 105], Provean [106], and GERP [107]
401 scores for deleteriousness, as well as ancestral allele state and synonymous annotations and for
402 all mutations in coding regions.

403 PolyPhen 2 generates three deleteriousness categories: Probably Damaging, Possible
404 Damaging, and Benign. If a mutation has more than one PolyPhen2 classification (e.g. Benign
405 and Probably Damaging), it is reassigned to have only the most damaging category of the group.
406 All mutations that have a PolyPhen 2 prediction or that are synonymous, are then pooled into two
407 separate categories: “damaging” and “benign.” All Probably Damaging or Possibly Damaging
408 mutations are pooled into the “damaging” category, and all Benign and synonymous mutations are
409 pooled into the “benign” category.

410 SIFT generates two deleteriousness categories, Intolerant and Tolerant, which we relabel
411 “damaging” and “benign.” If a mutation has more than one SIFT classification, it is reassigned to
412 have only the most damaging category of the group.

413 Provean generates two deleteriousness categories, Deleterious and Neutral, which we
414 relabel “damaging” and “benign.” If a mutation has more than one Provean classification, it is
415 reassigned to have only the most damaging category of the group.

416 GERP generates a numerical score at a given locus where a higher score indicates more
417 deleteriousness for a derived allele at that locus. Here we focus on derived alleles that are very
418 likely to be deleterious and combine all derived mutations at sites with $GERP \geq 6$ into the
419 category “damaging.” We form our “benign” category with all derived mutations with $GERP \leq 2$.

420

421
422
423

Table 1. The number of deleterious alleles per megabase partitioned by population and local ancestry background.

| | AFR ($p = 0.160$) | EUR ($p = 0.452$) | NAM*** ($p = 3.314 \times 10^{-7}$) | EUAF** ($p = 1.131 \times 10^{-3}$) | EUNA ($p = 0.123$) | AFNA** ($p = 4.392 \times 10^{-3}$) |
|--------------------------------------|----------------------------------|----------------------------------|--|--|----------------------------------|--|
| AA*** ($p < 2 \times 10^{-16}$) | 0.335 (1.642×10^6) | 0.284 (1.009×10^5) | 0.237 (8.648×10^2) | 0.311 (7.943×10^5) | 0.280 (2.491×10^4) | 0.315 (8.364×10^4) |
| PR*** ($p < 2 \times 10^{-16}$) | 0.337 (1.603×10^5) | 0.282 (1.064×10^6) | 0.275 (5.395×10^4) | 0.313 (7.517×10^5) | 0.286 (4.912×10^5) | 0.308 (1.700×10^5) |
| MX*** ($p < 2 \times 10^{-16}$) | 0.341 (7.651×10^3) | 0.282 (4.585×10^5) | 0.286 (8.275×10^5) | 0.317 (1.154×10^5) | 0.287 (1.142×10^6) | 0.314 (1.393×10^5) |

424 Total number of megabases, summed across all individuals, in parentheses. A significant
425 difference (Pearson's Chi-squared test, p-value in parentheses) across populations for a given
426 ancestry background is denoted at the beginning of a column. A significant difference across
427 ancestry backgrounds for a given population (Pearson's Chi-squared test, p-value in parentheses)
428 is denoted at the beginning of a row. Population codes: AA - African American, PR - Puerto Rican,
429 MX - Mexican American. Local ancestry codes: AFR - Homozygous African, EUR - Homozygous
430 European, NAM - Homozygous Native American, EUAF - Heterozygous European/African, EUNA
431 - Heterozygous European/Native American, AFNA - Heterozygous African/Native American. * $p <$
432 0.05 , ** $p < 0.01$, *** $p < 0.001$.

433
434
435
436

Table 2. Regression coefficients inferred for the analyses shown in Fig 4 with p-values in parentheses.

| ROH Class | β_0 (p-value) | β_1 (p-value) | β_2 (p-value) | β_3 (p-value) |
|--------------|---|---------------------------------------|---|--|
| All | *** 3.122×10^{-2} ($< 2 \times 10^{-16}$) | ***1.460 ($< 2 \times 10^{-16}$) | ***0.180 ($< 2 \times 10^{-16}$) | 1.807×10^{-2} (0.0671) |
| Long | 1.059×10^{-3} (0.508) | ***1.429 ($< 2 \times 10^{-16}$) | *** 5.335×10^{-2} ($< 2 \times 10^{-16}$) | ***0.229 ($< 2 \times 10^{-16}$) |
| Medium | *** 8.510×10^{-3} ($< 3.86 \times 10^{-5}$) | ***1.584 ($< 2 \times 10^{-16}$) | *** 7.012×10^{-2} ($< 2 \times 10^{-16}$) | * 5.695×10^{-2} (0.0173) |
| Short | *** 1.265×10^{-2} (4.61×10^{-7}) | ***1.424 ($< 2 \times 10^{-16}$) | *** 4.810×10^{-2} ($< 2 \times 10^{-16}$) | ***-0.428 (1.10×10^{-8}) |

437
438

* $p < 0.05$, ** $p < 0.01$, *** $p < 0.001$.

439
440
441

Table 3. Regression coefficients inferred for the analyses shown in Fig 5 and S1 Fig with p-values in parentheses.

| ROH Class | Ancestral Haplotype | β_0 (p-value) | β_1 (p-value) | β_2 (p-value) | β_3 (p-value) |
|-----------|---------------------|---|---------------------------------------|---|--|
| All | NAM | *** 3.455×10^{-3} (3.18×10^{-4}) | ***1.594 ($< 2 \times 10^{-16}$) | *** 7.369×10^{-3} (5.87×10^{-8}) | ***0.510 ($< 2 \times 10^{-16}$) |
| | EUR | -1.205×10^{-3} (0.2081) | ***1.546 ($< 2 \times 10^{-16}$) | 2.497×10^{-3} (6.52×10^{-2}) | ***0.648 ($< 2 \times 10^{-16}$) |
| | AFR | * 1.308×10^{-3} (3.11×10^{-2}) | ***1.743 ($< 2 \times 10^{-16}$) | -1.210×10^{-3} (0.1587) | ***1.214 ($< 2 \times 10^{-16}$) |
| Long | NAM | ** 1.989×10^{-3} (3.38×10^{-3}) | ***1.545 ($< 2 \times 10^{-16}$) | *** 4.192×10^{-3} (1.28×10^{-5}) | ***0.604 ($< 2 \times 10^{-16}$) |
| | EUR | -3.026×10^{-4} (0.623) | ***1.403 ($< 2 \times 10^{-16}$) | 1.260×10^{-3} (0.148) | ***0.624 ($< 2 \times 10^{-16}$) |
| | AFR | 5.324×10^{-4} (0.286) | ***1.610 ($< 2 \times 10^{-16}$) | 1.134×10^{-4} (0.872) | ***1.265 ($< 2 \times 10^{-16}$) |
| Medium | NAM | * 1.237×10^{-3} (1.661×10^{-2}) | ***1.679 ($< 2 \times 10^{-16}$) | ** 2.325×10^{-3} (1.46×10^{-3}) | ***0.421 ($< 2 \times 10^{-16}$) |
| | EUR | -5.614×10^{-4} (0.340) | ***1.651 ($< 2 \times 10^{-16}$) | 8.918×10^{-4} (0.284) | ***0.684 ($< 2 \times 10^{-16}$) |
| | AFR | 4.961×10^{-4} (0.246) | ***1.797 ($< 2 \times 10^{-16}$) | -1.001×10^{-3} (0.0979) | ***1.217 ($< 2 \times 10^{-16}$) |
| Short | NAM | 2.711×10^{-4} (0.259) | ***1.594 ($< 2 \times 10^{-16}$) | ** 1.073×10^{-3} (1.61×10^{-3}) | ***0.244 (1.27×10^{-13}) |
| | EUR | -1.125×10^{-4} (0.720) | ***1.665 ($< 2 \times 10^{-16}$) | 4.023×10^{-4} (0.364) | ***0.609 ($< 2 \times 10^{-16}$) |
| | AFR | 2.349×10^{-4} (0.430) | ***1.881 ($< 2 \times 10^{-16}$) | -2.568×10^{-4} (0.542) | ***1.116 ($< 2 \times 10^{-16}$) |

442 * $p < 0.05$, ** $p < 0.01$, *** $p < 0.001$.

443 **Table 4. Regression coefficients inferred for the analyses shown in Fig 6 and S2 Fig with p-**
 444 **values in parentheses.**

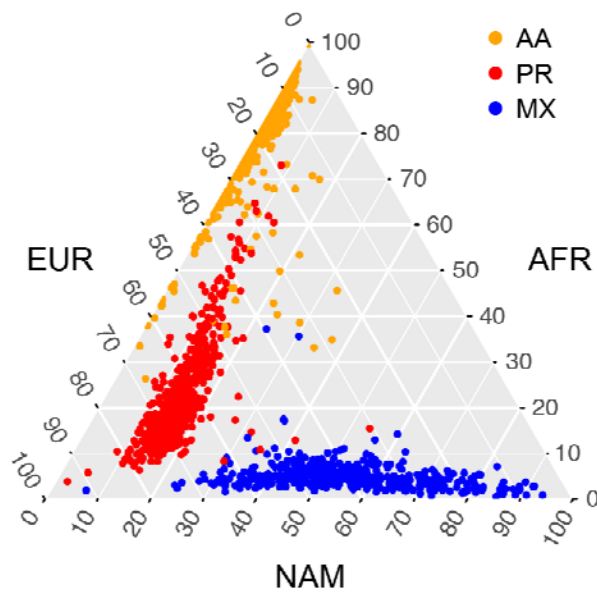
445

| ROH Class | β_0 (p-value) | β_1 (p-value) | β_2 (p-value) | β_3 (p-value) | β_4 (p-value) | β_5 (p-value) |
|-----------|------------------------|------------------------|------------------------|------------------------|------------------------|------------------------|
|-----------|------------------------|------------------------|------------------------|------------------------|------------------------|------------------------|

| | | | | | | |
|--------|-----|-----|-----|-----|-----|-----|
| All | () | () | () | () | () | () |
| Long | () | () | () | () | () | () |
| Medium | () | () | () | () | () | () |
| Short | () | () | () | () | () | () |

446
447

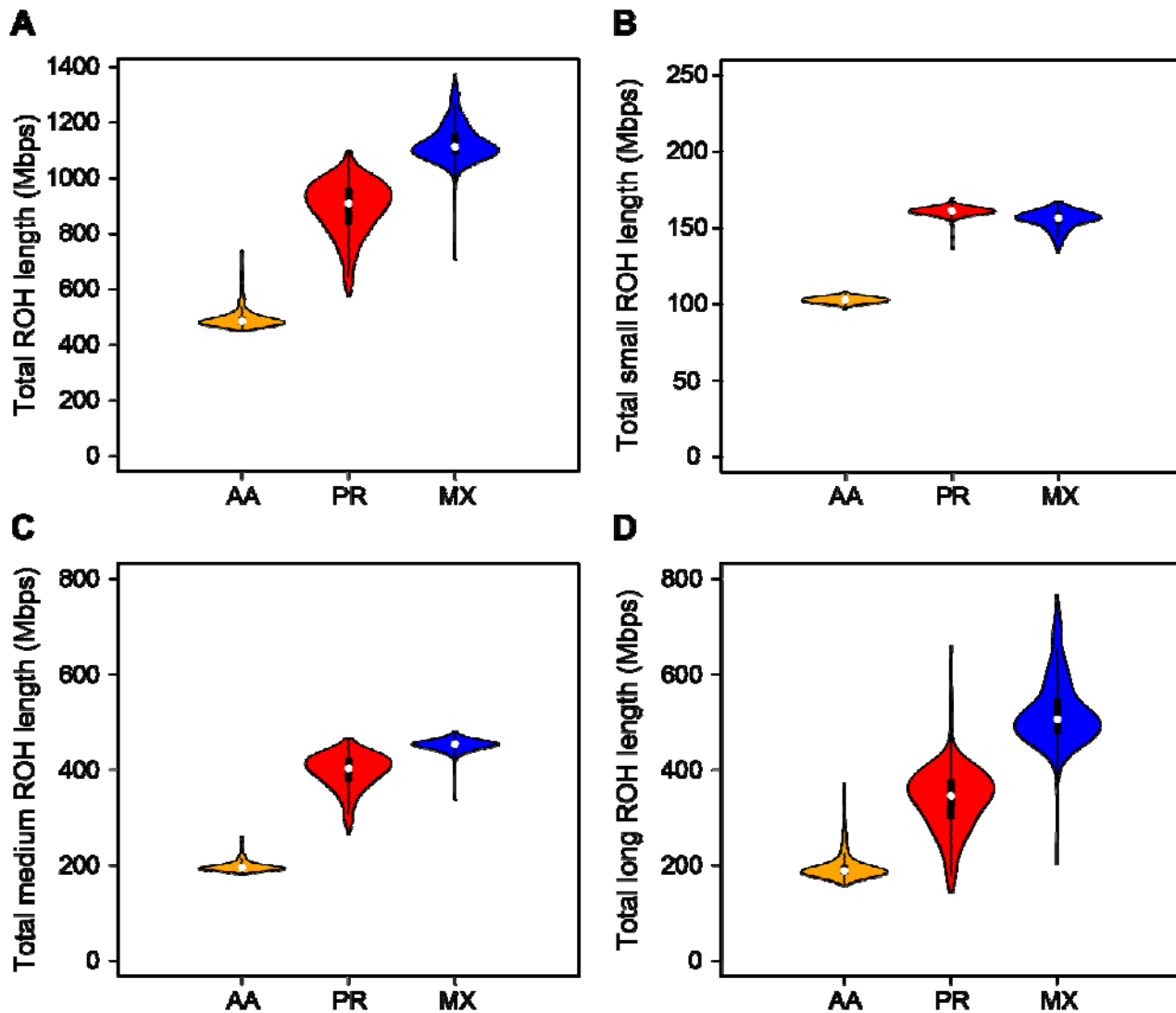
* $p < 0.05$, ** $p < 0.01$, *** $p < 0.001$.



448
449
450
451
452
453
454

Fig 1. A ternary plot of global ancestry proportions.

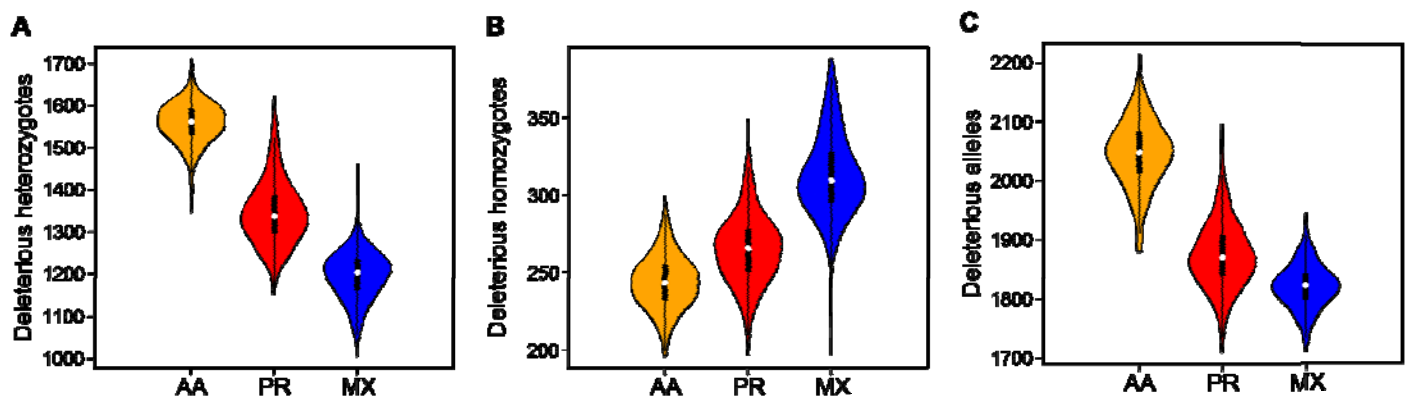
Each point represents a single individual, with their global ancestry proportions shown on each of the three axes (European, EUR; African, AFR; and Native American, NAM). Individuals are colored based on their reported ethnicity, with African Americans (AA) colored orange, Puerto Ricans (PR) colored red, and Mexican Americans (MX) colored blue.



455
456
457
458
459

Fig 2. The distribution of summed ROH lengths across size classes.

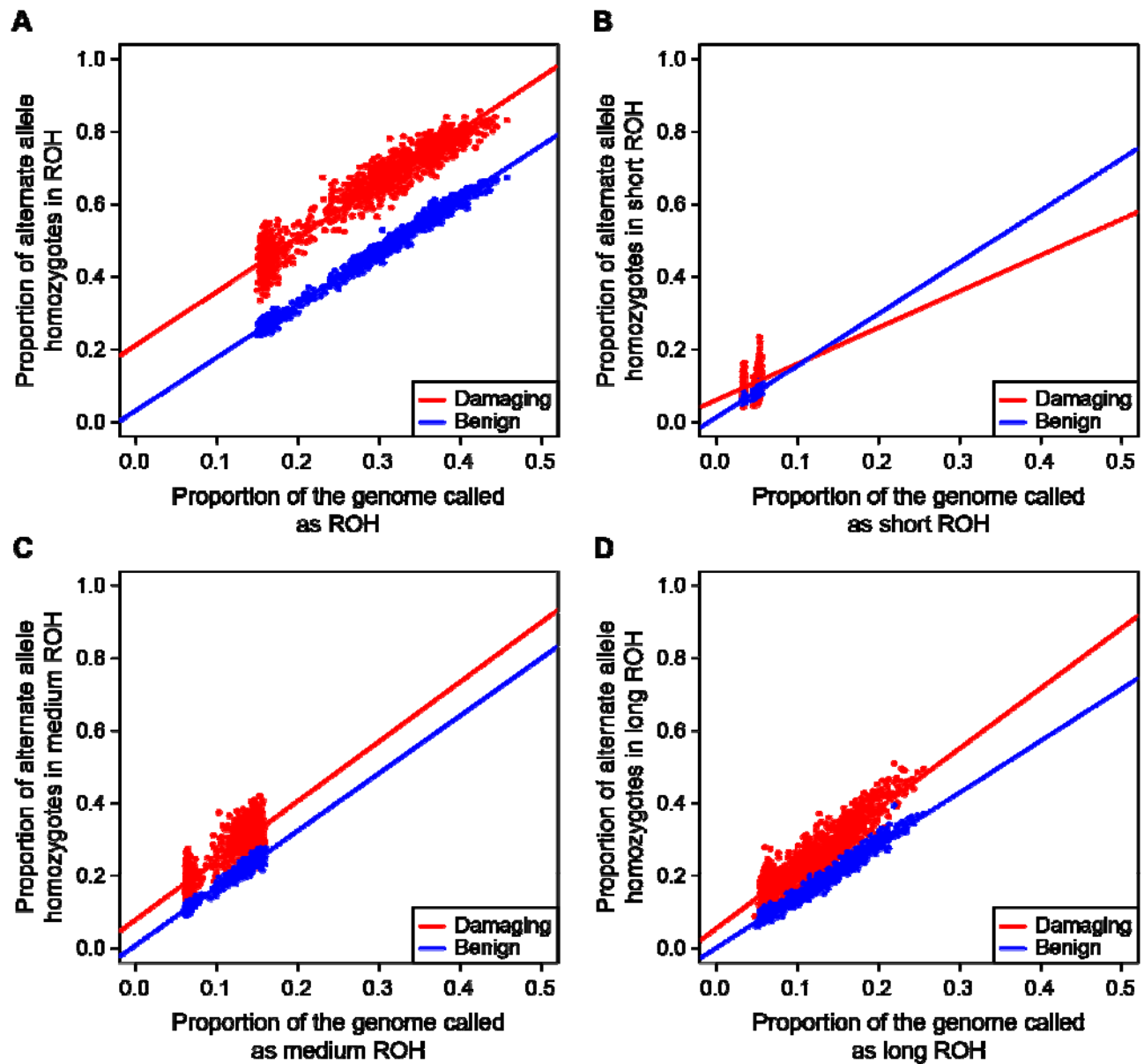
(A) all ROH, (B) short ROH, (C) medium ROH, and (D) long ROH. AA – African American, PR – Puerto Rican, MX – Mexican American.



460
461
462
463
464
465

Fig 3. The distribution of deleterious alleles across populations.

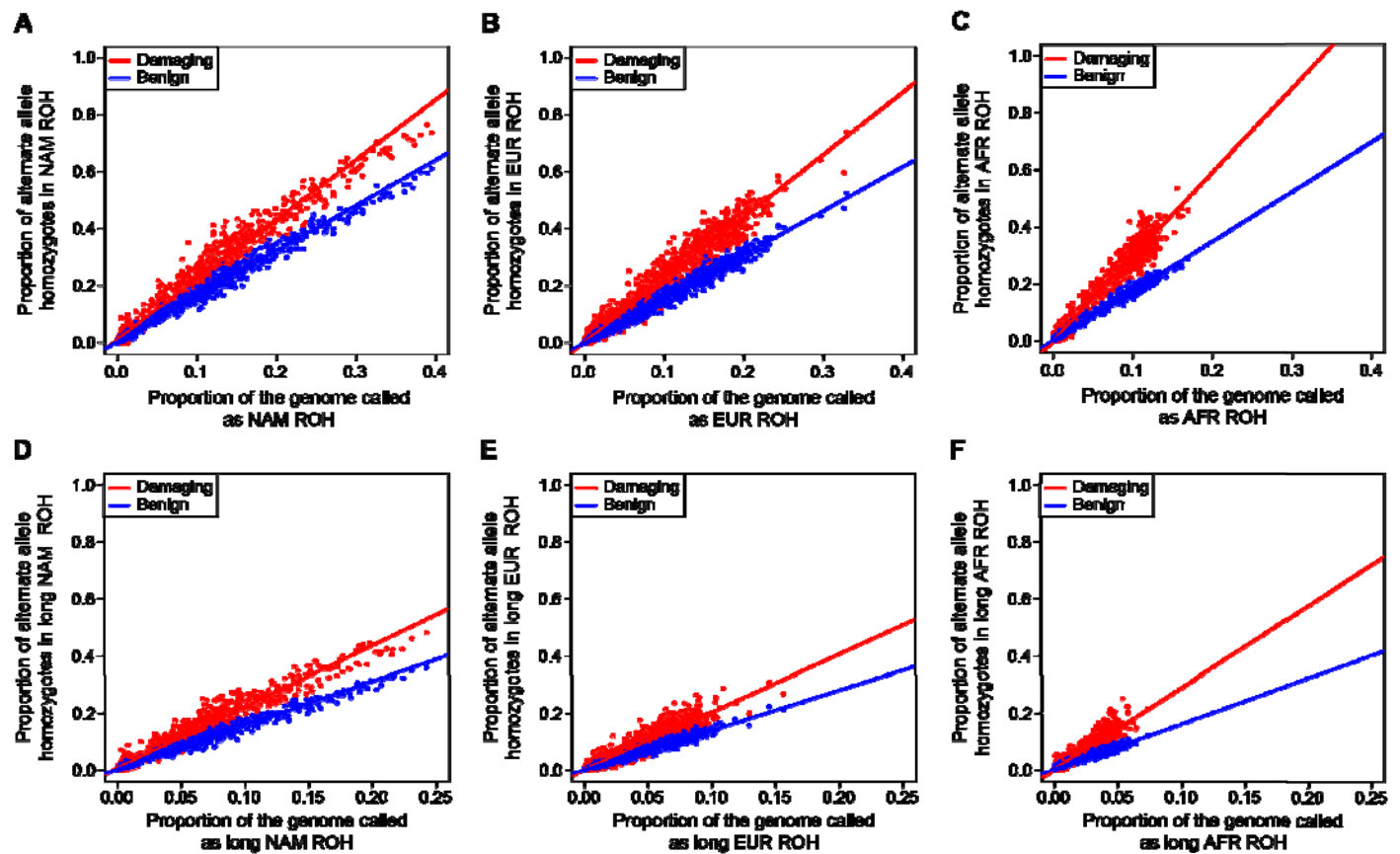
The number of (A) deleterious heterozygotes, (B) deleterious homozygotes, and (C) total deleterious alleles per individual using Polyphen2 classifications. AA – African American, PR – Puerto Rican, MX – Mexican American.



466
467
468
469
470

Fig 4. Deleterious and benign homozygotes in ROH classes.

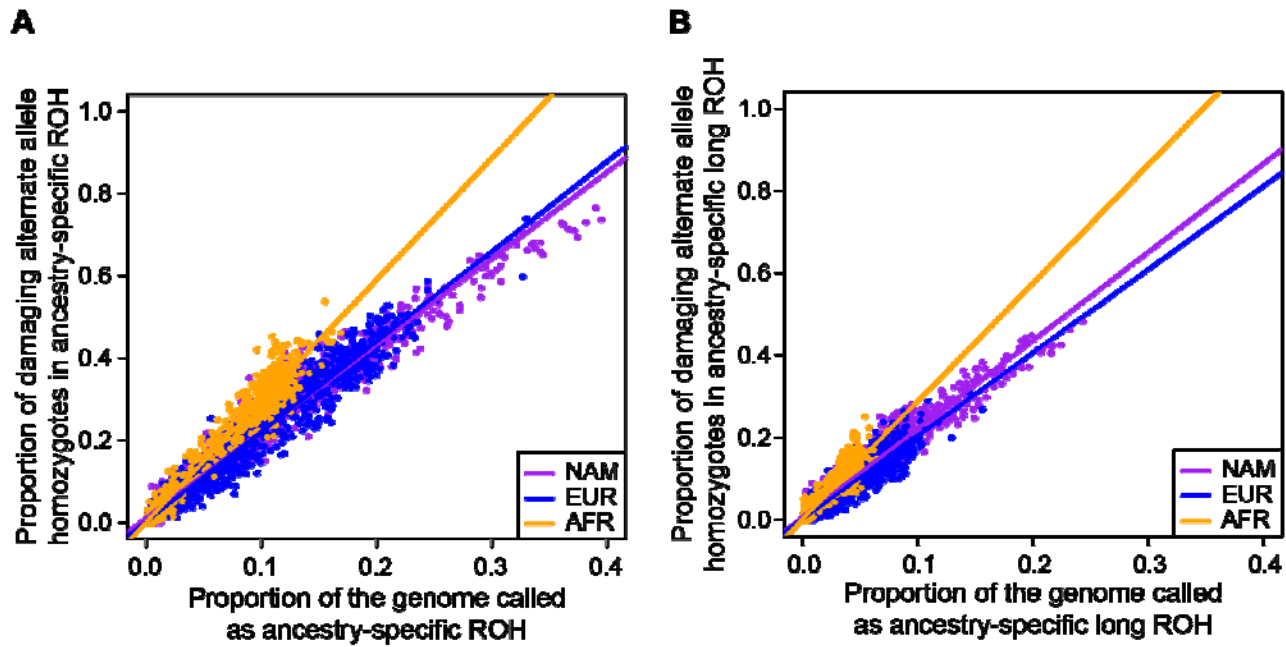
The proportion of damaging (red) and benign (blue) homozygotes falling in ROH of different size classes: (A) all ROH, (B) short ROH, (C) medium ROH, and (D) long ROH.



471
472
473
474
475
476
477
478
479
480

Fig 5. Deleterious and benign homozygotes in ROH classes separated by ancestry.

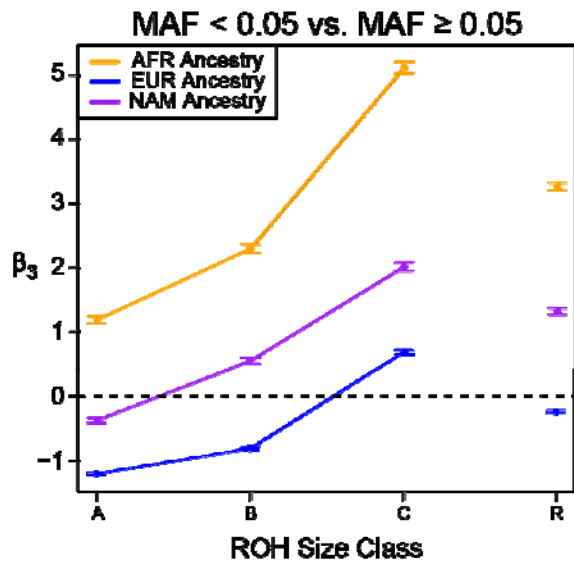
The proportion of damaging (red) and benign (blue) homozygotes falling in ROH comprised of different ancestral haplotypes and size classes: (A) all NAM ROH, (B) all EUR ROH, (C) all AFR ROH, (D) long NAM ROH, (E) long EUR ROH, and (F) long AFR ROH. EUR – European, AFR – African, and NAM – Native American.



481
482
483
484
485
486

Fig 6. Deleterious homozygotes in ROH classes compared across ancestry.

A direct comparison of the proportion of damaging homozygotes falling in ROH comprised of different ancestral haplotypes for (A) all ROH and (B) long ROH. EUR – European, colored blue; AFR – African, colored orange; and NAM – Native American, colored purple.



487
488
489
490
491
492
493
494
495

Fig 7. Enrichment of low-frequency variants across ROH sizes.

The difference in rate of gain of low-frequency minor allele homozygotes () compared to common minor allele homozygotes (; from regression analysis). ROH size classes: A – short, B – medium, C – long, R – all sizes. EUR – European, colored blue; AFR – African, colored orange; and NAM – Native American, colored purple. Error bars represent standard error of the regression coefficient.

496
497

498 SUPPORTING INFORMATION

499 **S1 Fig. Deleterious versus benign homozygotes by ancestry for medium and small ROH.**

500 The proportion of damaging (red) and benign (blue) homozygotes falling in ROH comprised of
501 different ancestral haplotypes and size classes: (A) medium NAM ROH, (B) medium EUR ROH,
502 (C) medium AFR ROH, (D) short NAM ROH, (E) short EUR ROH, and (F) short AFR ROH. EUR –
503 European, AFR – African, and NAM – Native American.

504

505 **S2 Fig. Comparison of deleterious homozygotes between ancestries for medium and small** 506 **ROH.**

507 A direct comparison of the proportion of damaging homozygotes falling in ROH comprised of
508 different ancestral haplotypes for (A) medium ROH and (B) short ROH. EUR – European, colored
509 blue; AFR – African, colored orange; and NAM – Native American, colored purple.

510

511 **S3 Fig. Regression coefficients for analyses with other deleteriousness classifications.**

512 The difference in slopes (β_3 coefficients) between deleterious and benign categories across ROH
513 size classes from re-analyses of the data using different deleteriousness classification schemes.
514 (A) SIFT, (B) Provean, (C) GERP, (D) SIFT only with derived alleles, (E) Provean only with
515 derived alleles, (F) Polyphen 2 only with derived alleles. ROH size classes: A – short, B –
516 medium, C – long, R – all sizes. EUR – European, colored blue; AFR – African, colored orange;
517 and NAM – Native American, colored purple.

518

519 **S4 Fig. Replication of findings using 1000 genomes data.**

520 The identical analysis from Fig 4A-C except using the six admixed populations from the 1000
521 Genomes Project and CADD scores. (A) Native American ancestry, (B) European Ancestry, (C)
522 African Ancestry.

523

524 **S5 Fig. The distribution of polarized Polyphen2 deleterious alleles across populations.**

525 The number of (A) deleterious heterozygotes, (B) deleterious homozygotes, and (C) total
526 deleterious alleles per individual using polarized Polyphen2 classifications. AA – African
527 American, PR – Puerto Rican, MX – Mexican American.

528

529 **S6 Fig. The distribution of SIFT deleterious alleles across populations.**

530 The number of (A) deleterious heterozygotes, (B) deleterious homozygotes, and (C) total
531 deleterious alleles per individual using SIFT classifications. AA – African American, PR – Puerto
532 Rican, MX – Mexican American.

533

534 **S7 Fig. The distribution of polarized SIFT deleterious alleles across populations.**

535 The number of (A) deleterious heterozygotes, (B) deleterious homozygotes, and (C) total
536 deleterious alleles per individual using polarized SIFT classifications. AA – African American, PR –
537 Puerto Rican, MX – Mexican American.

538

539 **S8 Fig. The distribution of Provean deleterious alleles across populations.**

540 The number of (A) deleterious heterozygotes, (B) deleterious homozygotes, and (C) total
541 deleterious alleles per individual using Provean classifications. AA – African American, PR –
542 Puerto Rican, MX – Mexican American.

543

544 **S9 Fig. The distribution of polarized Provean deleterious alleles across populations.**

545 The number of (A) deleterious heterozygotes, (B) deleterious homozygotes, and (C) total
546 deleterious alleles per individual using polarized Provean classifications. AA – African American,
547 PR – Puerto Rican, MX – Mexican American.

548

549 **S10 Fig. The distribution of GERP deleterious alleles across populations.**

550 The number of (A) deleterious heterozygotes, (B) deleterious homozygotes, and (C) total
551 deleterious alleles per individual using GERP classifications. AA – African American, PR – Puerto
552 Rican, MX – Mexican American.

553

554 **S1 Text. Processing of 1000 genomes data.**

555

556 **References**

- 557 1. Ceballos FC, Joshi PK, Clark DW, Ramsay M, Wilson JF. Runs of homozygosity: windows into
558 population history and trait architecture. *Nature Reviews Genetics*. 2018.
- 559 2. Broman KW, Weber JL. Long homozygous chromosomal segments in reference families from
560 the centre d'Etude du polymorphisme humain. *Am J Hum Genet*. 1999;65(6):1493-500. Epub
561 1999/12/01. doi: 10.1086/302661. PubMed PMID: 10577902; PubMed Central PMCID:
562 PMCPMC1288359.
- 563 3. Gibson J, Morton NE, Collins A. Extended tracts of homozygosity in outbred human
564 populations. *Hum Mol Genet*. 2006;15(5):789-95. Epub 2006/01/27. doi: 10.1093/hmg/ddi493.
565 PubMed PMID: 16436455.
- 566 4. McQuillan R, Leutenegger AL, Abdel-Rahman R, Franklin CS, Pericic M, Barac-Lauc L, et al. Runs
567 of homozygosity in European populations. *Am J Hum Genet*. 2008;83(3):359-72. Epub 2008/09/02.
568 doi: 10.1016/j.ajhg.2008.08.007. PubMed PMID: 18760389; PubMed Central PMCID:
569 PMCPMC2556426.
- 570 5. Kirin M, McQuillan R, Franklin CS, Campbell H, McKeigue PM, Wilson JF. Genomic runs of
571 homozygosity record population history and consanguinity. *PLoS One*. 2010;5(11):e13996. Epub
572 2010/11/19. doi: 10.1371/journal.pone.0013996. PubMed PMID: 21085596; PubMed Central PMCID:
573 PMCPMC2981575.
- 574 6. Nothnagel M, Lu TT, Kayser M, Krawczak M. Genomic and geographic distribution of SNP-
575 defined runs of homozygosity in Europeans. *Hum Mol Genet*. 2010;19(15):2927-35. Epub
576 2010/05/14. doi: 10.1093/hmg/ddq198. PubMed PMID: 20462934.
- 577 7. Pemberton TJ, Absher D, Feldman MW, Myers RM, Rosenberg NA, Li JZ. Genomic patterns of
578 homozygosity in worldwide human populations. *Am J Hum Genet*. 2012;91(2):275-92. Epub
579 2012/08/14. doi: 10.1016/j.ajhg.2012.06.014. PubMed PMID: 22883143; PubMed Central PMCID:
580 PMCPMC3415543.
- 581 8. Blant A, Kwong M, Szpiech ZA, Pemberton TJ. Weighted likelihood inference of genomic
582 autozygosity patterns in dense genotype data. *BMC Genomics*. 2017;18(1):928. Epub 2017/12/02.
583 doi: 10.1186/s12864-017-4312-3. PubMed PMID: 29191164; PubMed Central PMCID:
584 PMCPMC5709839.
- 585 9. Ben Halim N, Nagara M, Regnault B, Hsouna S, Lasram K, Kefi R, et al. Estimation of Recent and
586 Ancient Inbreeding in a Small Endogamous Tunisian Community Through Genomic Runs of
587 Homozygosity. *Annals of Human Genetics*. 2015;79(6):402-17. doi: 10.1111/ahg.12131. PubMed
588 PMID: WOS:000365399000003.
- 589 10. Kardos M, Luikart G, Allendorf FW. Measuring individual inbreeding in the age of genomics:
590 marker-based measures are better than pedigrees. *Heredity (Edinb)*. 2015;115(1):63-72. Epub
591 2015/06/11. doi: 10.1038/hdy.2015.17. PubMed PMID: 26059970; PubMed Central PMCID:
592 PMCPMC4815495.

- 593 11. Mastrangelo S, Tolone M, Di Gerlando R, Fontanesi L, Sardina MT, Portolano B. Genomic
594 inbreeding estimation in small populations: evaluation of runs of homozygosity in three local dairy
595 cattle breeds. *Animal*. 2016;10(5):746-54. doi: 10.1017/S1751731115002943. PubMed PMID:
596 WOS:000377125600003.
- 597 12. Kang JTL, Goldberg A, Edge MD, Behar DM, Rosenberg NA. Consanguinity Rates Predict Long
598 Runs of Homozygosity in Jewish Populations. *Hum Hered*. 2016;82(3-4):87-102. Epub 2017/09/15.
599 doi: 10.1159/000478897. PubMed PMID: 28910803; PubMed Central PMCID: PMC5698150.
- 600 13. Meyer M, Kircher M, Gansauge MT, Li H, Racimo F, Mallick S, et al. A High-Coverage Genome
601 Sequence from an Archaic Denisovan Individual. *Science*. 2012;338(6104):222-6. doi:
602 10.1126/science.1224344. PubMed PMID: WOS:000309712300037.
- 603 14. Castellano S, Parra G, Sanchez-Quinto FA, Racimo F, Kuhlwilm M, Kircher M, et al. Patterns of
604 coding variation in the complete exomes of three Neandertals. *P Natl Acad Sci USA*.
605 2014;111(18):6666-71. doi: 10.1073/pnas.1405138111. PubMed PMID: WOS:000335477300045.
- 606 15. Prufer K, Racimo F, Patterson N, Jay F, Sankararaman S, Sawyer S, et al. The complete genome
607 sequence of a Neanderthal from the Altai Mountains. *Nature*. 2014;505(7481):43-+. doi:
608 10.1038/nature12886. PubMed PMID: WOS:000329163300020.
- 609 16. Gamba C, Jones ER, Teasdale MD, McLaughlin RL, Gonzalez-Fortes G, Mattiangeli V, et al.
610 Genome flux and stasis in a five millennium transect of European prehistory. *Nature Communications*.
611 2014;5. doi: ARTN 5257
612 10.1038/ncomms6257. PubMed PMID: WOS:000343985400006.
- 613 17. Prado-Martinez J, Sudmant PH, Kidd JM, Li H, Kelley JL, Lorente-Galdos B, et al. Great ape
614 genetic diversity and population history. *Nature*. 2013;499(7459):471-5. doi: 10.1038/nature12228.
615 PubMed PMID: WOS:000322157900039.
- 616 18. Xue YL, Prado-Martinez J, Sudmant PH, Narasimhan V, Ayub Q, Szpak M, et al. Mountain gorilla
617 genomes reveal the impact of long-term population decline and inbreeding. *Science*.
618 2015;348(6231):242-5. doi: 10.1126/science.aaa3952. PubMed PMID: WOS:000352613700048.
- 619 19. Palkopoulou E, Mallick S, Skoglund P, Enk J, Rohland N, Li H, et al. Complete Genomes Reveal
620 Signatures of Demographic and Genetic Declines in the Woolly Mammoth. *Current Biology*.
621 2015;25(10):1395-400. doi: 10.1016/j.cub.2015.04.007. PubMed PMID: WOS:000354785900035.
- 622 20. Curik I, Ferencakovic M, Solkner J. Inbreeding and runs of homozygosity: A possible solution to
623 an old problem. *Livest Sci*. 2014;166:26-34. doi: 10.1016/j.livsci.2014.05.034. PubMed PMID:
624 WOS:000340994000005.
- 625 21. Zhang Q, Guldbbrandtsen B, Bosse M, Lund MS, Sahana G. Runs of homozygosity and
626 distribution of functional variants in the cattle genome. *BMC Genomics*. 2015;16:542. Epub
627 2015/07/23. doi: 10.1186/s12864-015-1715-x. PubMed PMID: 26198692; PubMed Central PMCID:
628 PMC4508970.
- 629 22. Howard JT, Tiezzi F, Huang Y, Gray KA, Maltecca C. Characterization and management of long
630 runs of homozygosity in parental nucleus lines and their associated crossbred progeny. *Genet Sel*
631 *Evol*. 2016;48. doi: ARTN 91
632 10.1186/s12711-016-0269-y. PubMed PMID: WOS:000388541600002.
- 633 23. Manunza A, Noce A, Serradilla JM, Goyache F, Martinez A, Capote J, et al. A genome-wide
634 perspective about the diversity and demographic history of seven Spanish goat breeds. *Genet Sel Evol*.
635 2016;48. doi: ARTN 52
636 10.1186/s12711-016-0229-6. PubMed PMID: WOS:000381071000001.
- 637 24. Gurgul A, Szmatola T, Topolski P, Jasielczuk I, Zukowski K, Bugno-Poniewierska M. The use of
638 runs of homozygosity for estimation of recent inbreeding in Holstein cattle. *J Appl Genet*.
639 2016;57(4):527-30. doi: 10.1007/s13353-016-0337-6. PubMed PMID: WOS:000385423900013.

- 640 25. Peripolli E, Stafuzza NB, Munari DP, Lima ALF, Irgang R, Machado MA, et al. Assessment of runs
641 of homozygosity islands and estimates of genomic inbreeding in Gyr (*Bos indicus*) dairy cattle. *Bmc*
642 *Genomics*. 2018;19. doi: ARTN 34
643 10.1186/s12864-017-4365-3. PubMed PMID: WOS:000419680000001.
- 644 26. Forutan M, Mahyari SA, Baes C, Melzer N, Schenkel FS, Sargolzaei M. Inbreeding and runs of
645 homozygosity before and after genomic selection in North American Holstein cattle. *Bmc Genomics*.
646 2018;19. doi: ARTN 98
647 10.1186/s12864-018-4453-z. PubMed PMID: WOS:000423444300001.
- 648 27. Kardos M, Qvarnstrom A, Ellegren H. Inferring Individual Inbreeding and Demographic History
649 from Segments of Identity by Descent in *Ficedula Flycatcher* Genome Sequences. *Genetics*.
650 2017;205(3):1319-34. doi: 10.1534/genetics.116.198861. PubMed PMID: WOS:000395807200022.
- 651 28. Bortoluzzi C, Crooijmans R, Bosse M, Hiemstra SJ, Groenen MAM, Megens HJ. The effects of
652 recent changes in breeding preferences on maintaining traditional Dutch chicken genomic diversity.
653 *Heredity (Edinb)*. 2018. Epub 2018/03/29. doi: 10.1038/s41437-018-0072-3. PubMed PMID:
654 29588508.
- 655 29. Bertolini F, Gandolfi B, Kim ES, Haase B, Lyons LA, Rothschild MF. Evidence of selection
656 signatures that shape the Persian cat breed. *Mamm Genome*. 2016;27(3-4):144-55. doi:
657 10.1007/s00335-016-9623-1. PubMed PMID: WOS:000373308200005.
- 658 30. Boyko AR, Quignon P, Li L, Schoenebeck JJ, Degenhardt JD, Lohmueller KE, et al. A Simple
659 Genetic Architecture Underlies Morphological Variation in Dogs. *Plos Biol*. 2010;8(8). doi: ARTN
660 e1000451
661 10.1371/journal.pbio.1000451. PubMed PMID: WOS:000281464500009.
- 662 31. vonHoldt BM, Pollinger JP, Earl DA, Knowles JC, Boyko AR, Parker H, et al. A genome-wide
663 perspective on the evolutionary history of enigmatic wolf-like canids. *Genome Research*.
664 2011;21(8):1294-305. doi: 10.1101/gr.116301.110. PubMed PMID: WOS:000293335700009.
- 665 32. Pilot M, Dabrowski MJ, Hayrapetyan V, Yavruyan EG, Kopaliani N, Tsingarska E, et al. Genetic
666 Variability of the Grey Wolf *Canis lupus* in the Caucasus in Comparison with Europe and the Middle
667 East: Distinct or Intermediary Population? *Plos One*. 2014;9(4). doi: ARTN e93828
668 10.1371/journal.pone.0093828. PubMed PMID: WOS:000334160900054.
- 669 33. Friedenbergs SG, Meurs KM, Mackay TFC. Evaluation of artificial selection in Standard Poodles
670 using whole-genome sequencing. *Mamm Genome*. 2016;27(11-12):599-609. doi: 10.1007/s00335-
671 016-9660-9. PubMed PMID: WOS:000388682800007.
- 672 34. Metzger J, Pfahler S, Distl O. Variant detection and runs of homozygosity in next generation
673 sequencing data elucidate the genetic background of Lundehund syndrome. *Bmc Genomics*. 2016;17.
674 doi: ARTN 535
675 10.1186/s12864-016-2844-6. PubMed PMID: WOS:000381222500003.
- 676 35. Pedersen NC, Pooch AS, Liu H. A genetic assessment of the English bulldog. *Canine genetics and*
677 *epidemiology*. 2016;3(1):6.
- 678 36. Dreger DL, Davis BW, Cocco R, Sechi S, Di Cerbo A, Parker HG, et al. Commonalities in
679 Development of Pure Breeds and Population Isolates Revealed in the Genome of the Sardinian Foini's
680 Dog. *Genetics*. 2016;204(2):737-55. doi: 10.1534/genetics.116.192427. PubMed PMID:
681 WOS:000385871400028.
- 682 37. Wiener P, Sanchez-Molano E, Clements DN, Woolliams JA, Haskell MJ, Blott SC. Genomic data
683 illuminates demography, genetic structure and selection of a popular dog breed. *Bmc Genomics*.
684 2017;18. doi: ARTN 609
685 10.1186/s12864-017-3933-x. PubMed PMID: WOS:000408036300001.
- 686 38. Sams AJ, Boyko AR. Fine-scale resolution and analysis of runs of homozygosity in domestic
687 dogs. *bioRxiv*. 2018. doi: 10.1101/315770.

- 688 39. Kardos M, Akesson M, Fountain T, Flagstad O, Liberg O, Olason P, et al. Genomic consequences
689 of intensive inbreeding in an isolated wolf population. *Nat Ecol Evol.* 2018;2(1):124-31. Epub
690 2017/11/22. doi: 10.1038/s41559-017-0375-4. PubMed PMID: 29158554.
- 691 40. Johnson EC, Evans LM, Keller MC. Relationships between estimated autozygosity and complex
692 traits in the UK Biobank. *bioRxiv.* 2018. doi: 10.1101/291872.
- 693 41. Sheridan E, Wright J, Small N, Corry PC, Oddie S, Whibley C, et al. Risk factors for congenital
694 anomaly in a multiethnic birth cohort: an analysis of the Born in Bradford study. *Lancet.*
695 2013;382(9901):1350-9. Epub 2013/07/09. doi: 10.1016/S0140-6736(13)61132-0. PubMed PMID:
696 23830354.
- 697 42. Bittles AH. Consanguineous marriages and congenital anomalies. *Lancet.*
698 2013;382(9901):1316-7. Epub 2013/07/09. doi: 10.1016/S0140-6736(13)61503-2. PubMed PMID:
699 23830356.
- 700 43. Scott EM, Halees A, Itan Y, Spencer EG, He Y, Azab MA, et al. Characterization of Greater Middle
701 Eastern genetic variation for enhanced disease gene discovery. *Nat Genet.* 2016;48(9):1071-6. Epub
702 2016/07/19. doi: 10.1038/ng.3592. PubMed PMID: 27428751; PubMed Central PMCID:
703 PMC5019950.
- 704 44. Shami SA, Qaisar R, Bittles AH. Consanguinity and adult morbidity in Pakistan. *Lancet.*
705 1991;338(8772):954. Epub 1991/10/12. PubMed PMID: 1681304.
- 706 45. Puzyrev VP, Lemza SV, Nazarenko LP, Panphilov VI. Influence of genetic and demographic
707 factors on etiology and pathogenesis of chronic disease in north Siberian aborigines. *Arctic Med Res.*
708 1992;51(3):136-42. Epub 1992/07/01. PubMed PMID: 1503580.
- 709 46. Ismail J, Jafar TH, Jafary FH, White F, Faruqui AM, Chaturvedi N. Risk factors for non-fatal
710 myocardial infarction in young South Asian adults. *Heart.* 2004;90(3):259-63. Epub 2004/02/18.
711 PubMed PMID: 14966040; PubMed Central PMCID: PMC1768096.
- 712 47. Christofidou P, Nelson CP, Nikpay M, Qu L, Li M, Loley C, et al. Runs of Homozygosity:
713 Association with Coronary Artery Disease and Gene Expression in Monocytes and Macrophages. *Am J*
714 *Hum Genet.* 2015;97(2):228-37. Epub 2015/07/15. doi: 10.1016/j.ajhg.2015.06.001. PubMed PMID:
715 26166477; PubMed Central PMCID: PMC4573243.
- 716 48. Simpson JL, Martin AO, Elias S, Sarto GE, Dunn JK. Cancers of the breast and female genital
717 system: search for recessive genetic factors through analysis of human isolate. *Am J Obstet Gynecol.*
718 1981;141(6):629-36. Epub 1981/11/15. PubMed PMID: 7315892.
- 719 49. Lebel RR, Gallagher WB. Wisconsin consanguinity studies. II: Familial adenocarcinomatosis.
720 *Am J Med Genet.* 1989;33(1):1-6. Epub 1989/05/01. doi: 10.1002/ajmg.1320330102. PubMed PMID:
721 2750776.
- 722 50. Rudan I. Inbreeding and cancer incidence in human isolates. *Hum Biol.* 1999;71(2):173-87.
723 Epub 1999/05/01. PubMed PMID: 10222641.
- 724 51. Bacolod MD, Schemmann GS, Wang S, Shattock R, Giardina SF, Zeng Z, et al. The signatures of
725 autozygosity among patients with colorectal cancer. *Cancer Res.* 2008;68(8):2610-21. Epub
726 2008/04/01. doi: 10.1158/0008-5472.CAN-07-5250. PubMed PMID: 18375840; PubMed Central
727 PMCID: PMC4383032.
- 728 52. Ujvari B, Klaassen M, Raven N, Russell T, Vittecoq M, Hamede R, et al. Genetic diversity,
729 inbreeding and cancer. *Proc Biol Sci.* 2018;285(1875). Epub 2018/03/23. doi:
730 10.1098/rspb.2017.2589. PubMed PMID: 29563261; PubMed Central PMCID: PMC5897632.
- 731 53. Krieger H. Inbreeding effects on metrical traits in Northeastern Brazil. *Am J Hum Genet.*
732 1969;21(6):537-46. Epub 1969/11/01. PubMed PMID: 5365755; PubMed Central PMCID:
733 PMC1706491.
- 734 54. Hurwich BJ, Nubani N. Blood pressures in a highly inbred community--Abu Ghosh, Israel. 1.
735 Original survey. *Isr J Med Sci.* 1978;14(9):962-9. Epub 1978/09/01. PubMed PMID: 721424.

- 736 55. Saleh EA, Mahfouz AA, Tayel KY, Naguib MK, Bin-al-Shaikh NM. Hypertension and its
737 determinants among primary-school children in Kuwait: an epidemiological study. *East Mediterr*
738 *Health J.* 2000;6(2-3):333-7. Epub 2001/09/15. PubMed PMID: 11556020.
- 739 56. Rudan I, Smolej-Narancic N, Campbell H, Carothers A, Wright A, Janicijevic B, et al. Inbreeding
740 and the genetic complexity of human hypertension. *Genetics.* 2003;163(3):1011-21. Epub
741 2003/03/29. PubMed PMID: 12663539; PubMed Central PMCID: PMCPMC1462484.
- 742 57. Campbell H, Carothers AD, Rudan I, Hayward C, Biloglav Z, Barac L, et al. Effects of genome-
743 wide heterozygosity on a range of biomedically relevant human quantitative traits. *Hum Mol Genet.*
744 2007;16(2):233-41. Epub 2007/01/16. doi: 10.1093/hmg/ddl473. PubMed PMID: 17220173.
- 745 58. Keller MC, Miller G. Resolving the paradox of common, harmful, heritable mental disorders:
746 which evolutionary genetic models work best? *Behav Brain Sci.* 2006;29(4):385-404; discussion 5-52.
747 Epub 2006/11/11. doi: 10.1017/S0140525X06009095. PubMed PMID: 17094843.
- 748 59. Keller MC, Simonson MA, Ripke S, Neale BM, Gejman PV, Howrigan DP, et al. Runs of
749 homozygosity implicate autozygosity as a schizophrenia risk factor. *PLoS Genet.* 2012;8(4):e1002656.
750 Epub 2012/04/19. doi: 10.1371/journal.pgen.1002656. PubMed PMID: 22511889; PubMed Central
751 PMCID: PMCPMC3325203.
- 752 60. Gandin I, Faletra F, Faletra F, Carella M, Pecile V, Ferrero GB, et al. Excess of runs of
753 homozygosity is associated with severe cognitive impairment in intellectual disability. *Genet Med.*
754 2015;17(5):396-9. Epub 2014/09/19. doi: 10.1038/gim.2014.118. PubMed PMID: 25232855.
- 755 61. Mukherjee S, Guha S, Ikeda M, Iwata N, Malhotra AK, Pe'er I, et al. Excess of homozygosity in
756 the major histocompatibility complex in schizophrenia. *Hum Mol Genet.* 2014;23(22):6088-95. Epub
757 2014/06/20. doi: 10.1093/hmg/ddu308. PubMed PMID: 24943592; PubMed Central PMCID:
758 PMCPMC4204767.
- 759 62. Iourov IY, Vorsanova SG, Korostelev SA, Zelenova MA, Yurov YB. Long contiguous stretches of
760 homozygosity spanning shortly the imprinted loci are associated with intellectual disability, autism
761 and/or epilepsy. *Mol Cytogenet.* 2015;8:77. Epub 2015/10/20. doi: 10.1186/s13039-015-0182-z.
762 PubMed PMID: 26478745; PubMed Central PMCID: PMCPMC4608298.
- 763 63. Ghani M, Reitz C, Cheng R, Vardarajan BN, Jun G, Sato C, et al. Association of Long Runs of
764 Homozygosity With Alzheimer Disease Among African American Individuals. *JAMA Neurol.*
765 2015;72(11):1313-23. Epub 2015/09/15. doi: 10.1001/jamaneurol.2015.1700. PubMed PMID:
766 26366463; PubMed Central PMCID: PMCPMC4641052.
- 767 64. McQuillan R, Eklund N, Pirastu N, Kuningas M, McEvoy BP, Esko T, et al. Evidence of inbreeding
768 depression on human height. *PLoS Genet.* 2012;8(7):e1002655. Epub 2012/07/26. doi:
769 10.1371/journal.pgen.1002655. PubMed PMID: 22829771; PubMed Central PMCID:
770 PMCPMC3400549.
- 771 65. Joshi PK, Esko T, Mattsson H, Eklund N, Gandin I, Nutile T, et al. Directional dominance on
772 stature and cognition in diverse human populations. *Nature.* 2015;523(7561):459-62. Epub
773 2015/07/02. doi: 10.1038/nature14618. PubMed PMID: 26131930; PubMed Central PMCID:
774 PMCPMC4516141.
- 775 66. Lyons EJ, Frodsham AJ, Zhang L, Hill AV, Amos W. Consanguinity and susceptibility to
776 infectious diseases in humans. *Biol Lett.* 2009;5(4):574-6. Epub 2009/03/28. doi:
777 10.1098/rsbl.2009.0133. PubMed PMID: 19324620; PubMed Central PMCID: PMCPMC2684220.
- 778 67. Pritchard JK. Are rare variants responsible for susceptibility to complex diseases? *Am J Hum*
779 *Genet.* 2001;69(1):124-37. Epub 2001/06/19. doi: 10.1086/321272. PubMed PMID: 11404818;
780 PubMed Central PMCID: PMCPMC1226027.
- 781 68. Pritchard JK, Cox NJ. The allelic architecture of human disease genes: common disease-
782 common variant...or not? *Hum Mol Genet.* 2002;11(20):2417-23. Epub 2002/09/28. PubMed PMID:
783 12351577.

- 784 69. Carlson CS, Eberle MA, Kruglyak L, Nickerson DA. Mapping complex disease loci in whole-
785 genome association studies. *Nature*. 2004;429(6990):446-52. Epub 2004/05/28. doi:
786 10.1038/nature02623. PubMed PMID: 15164069.
- 787 70. Freimer N, Sabatti C. The use of pedigree, sib-pair and association studies of common diseases
788 for genetic mapping and epidemiology. *Nat Genet*. 2004;36(10):1045-51. Epub 2004/09/30. doi:
789 10.1038/ng1433. PubMed PMID: 15454942.
- 790 71. Boyle EA, Li YI, Pritchard JK. An Expanded View of Complex Traits: From Polygenic to
791 Omnigenic. *Cell*. 2017;169(7):1177-86. Epub 2017/06/18. doi: 10.1016/j.cell.2017.05.038. PubMed
792 PMID: 28622505; PubMed Central PMCID: PMC5536862.
- 793 72. Reich DE, Lander ES. On the allelic spectrum of human disease. *Trends Genet*. 2001;17(9):502-
794 10. Epub 2001/08/30. PubMed PMID: 11525833.
- 795 73. Szpiech ZA, Xu J, Pemberton TJ, Peng W, Zollner S, Rosenberg NA, et al. Long runs of
796 homozygosity are enriched for deleterious variation. *Am J Hum Genet*. 2013;93(1):90-102. Epub
797 2013/06/12. doi: 10.1016/j.ajhg.2013.05.003. PubMed PMID: 23746547; PubMed Central PMCID:
798 PMC53710769.
- 799 74. Pemberton TJ, Szpiech ZA. Relationship between Deleterious Variation, Genomic Autozygosity,
800 and Disease Risk: Insights from The 1000 Genomes Project. *Am J Hum Genet*. 2018;102(4):658-75.
801 Epub 2018/03/20. doi: 10.1016/j.ajhg.2018.02.013. PubMed PMID: 29551419.
- 802 75. Colby SL, Ortman JM. Projections of the size and composition of the US population: 2014 to
803 2060: Population estimates and projections. 2017.
- 804 76. Popejoy AB, Fullerton SM. Genomics is failing on diversity. *Nature*. 2016;538(7624):161-4. doi:
805 DOI 10.1038/538161a. PubMed PMID: WOS:000386671000016.
- 806 77. Martin AR, Gignoux CR, Walters RK, Wojcik GL, Neale BM, Gravel S, et al. Human Demographic
807 History Impacts Genetic Risk Prediction across Diverse Populations. *Am J Hum Genet*.
808 2017;100(4):635-49. Epub 2017/04/04. doi: 10.1016/j.ajhg.2017.03.004. PubMed PMID: 28366442;
809 PubMed Central PMCID: PMC5384097.
- 810 78. Verdu P, Austerlitz F, Estoup A, Vitalis R, Georges M, Thery S, et al. Origins and genetic diversity
811 of pygmy hunter-gatherers from Western Central Africa. *Curr Biol*. 2009;19(4):312-8. Epub
812 2009/02/10. doi: 10.1016/j.cub.2008.12.049. PubMed PMID: 19200724.
- 813 79. Verdu P, Rosenberg NA. A general mechanistic model for admixture histories of hybrid
814 populations. *Genetics*. 2011;189(4):1413-26. Epub 2011/10/05. doi: 10.1534/genetics.111.132787.
815 PubMed PMID: 21968194; PubMed Central PMCID: PMC3241432.
- 816 80. Via M, Gignoux CR, Roth LA, Fejerman L, Galanter J, Choudhry S, et al. History shaped the
817 geographic distribution of genomic admixture on the island of Puerto Rico. *PLoS One*.
818 2011;6(1):e16513. Epub 2011/02/10. doi: 10.1371/journal.pone.0016513. PubMed PMID:
819 21304981; PubMed Central PMCID: PMC3031579.
- 820 81. Gravel S. Population genetics models of local ancestry. *Genetics*. 2012;191(2):607-19. Epub
821 2012/04/12. doi: 10.1534/genetics.112.139808. PubMed PMID: 22491189; PubMed Central PMCID:
822 PMC3374321.
- 823 82. Moreno-Estrada A, Gravel S, Zakharia F, McCauley JL, Byrnes JK, Gignoux CR, et al.
824 Reconstructing the population genetic history of the Caribbean. *PLoS Genet*. 2013;9(11):e1003925.
825 Epub 2013/11/19. doi: 10.1371/journal.pgen.1003925. PubMed PMID: 24244192; PubMed Central
826 PMCID: PMC3828151 Ancestry.com, 23andMe's "Roots into the Future" project, and Personalis,
827 Inc. He is on the medical advisory board of Invitae and Med-tek. None of these entities played any role
828 in the project or research results reported here.
- 829 83. Gravel S, Zakharia F, Moreno-Estrada A, Byrnes JK, Muzzio M, Rodriguez-Flores JL, et al.
830 Reconstructing Native American migrations from whole-genome and whole-exome data. *PLoS Genet*.
831 2013;9(12):e1004023. Epub 2014/01/05. doi: 10.1371/journal.pgen.1004023. PubMed PMID:
832 24385924; PubMed Central PMCID: PMC3873240.

- 833 84. Goldberg A, Verdu P, Rosenberg NA. Autosomal admixture levels are informative about sex
834 bias in admixed populations. *Genetics*. 2014;198(3):1209-29. Epub 2014/09/07. doi:
835 10.1534/genetics.114.166793. PubMed PMID: 25194159; PubMed Central PMCID: PMC4224161.
- 836 85. Verdu P, Pemberton TJ, Laurent R, Kemp BM, Gonzalez-Oliver A, Gorodezky C, et al. Patterns of
837 admixture and population structure in native populations of Northwest North America. *PLoS Genet*.
838 2014;10(8):e1004530. Epub 2014/08/15. doi: 10.1371/journal.pgen.1004530. PubMed PMID:
839 25122539; PubMed Central PMCID: PMC4133047.
- 840 86. Homburger JR, Moreno-Estrada A, Gignoux CR, Nelson D, Sanchez E, Ortiz-Tello P, et al.
841 Genomic Insights into the Ancestry and Demographic History of South America. *PLoS Genet*.
842 2015;11(12):e1005602. Epub 2015/12/05. doi: 10.1371/journal.pgen.1005602. PubMed PMID:
843 26636962; PubMed Central PMCID: PMC4670080.
- 844 87. Baharian S, Barakatt M, Gignoux CR, Shringarpure S, Errington J, Blot WJ, et al. The Great
845 Migration and African-American Genomic Diversity. *PLoS Genet*. 2016;12(5):e1006059. Epub
846 2016/05/28. doi: 10.1371/journal.pgen.1006059. PubMed PMID: 27232753; PubMed Central PMCID:
847 PMC4883799.
- 848 88. Browning SR, Browning BL, Daviglus ML, Durazo-Arvizu RA, Schneiderman N, Kaplan RC, et al.
849 Ancestry-specific recent effective population size in the Americas. *PLoS Genet*. 2018;14(5):e1007385.
850 Epub 2018/05/26. doi: 10.1371/journal.pgen.1007385. PubMed PMID: 29795556.
- 851 89. Zhu X, Tang H, Risch N. Admixture mapping and the role of population structure for localizing
852 disease genes. *Adv Genet*. 2008;60:547-69. Epub 2008/03/25. doi: 10.1016/S0065-2660(07)00419-
853 1. PubMed PMID: 18358332.
- 854 90. Basu A, Tang H, Arnett D, Gu CC, Mosley T, Kardia S, et al. Admixture mapping of quantitative
855 trait loci for BMI in African Americans: evidence for loci on chromosomes 3q, 5q, and 15q. *Obesity*
856 (Silver Spring). 2009;17(6):1226-31. Epub 2009/07/09. doi: 10.1038/oby.2009.24. PubMed PMID:
857 19584881; PubMed Central PMCID: PMC2929755.
- 858 91. Cheng CY, Kao WH, Patterson N, Tandon A, Haiman CA, Harris TB, et al. Admixture mapping of
859 15,280 African Americans identifies obesity susceptibility loci on chromosomes 5 and X. *PLoS Genet*.
860 2009;5(5):e1000490. Epub 2009/05/23. doi: 10.1371/journal.pgen.1000490. PubMed PMID:
861 19461885; PubMed Central PMCID: PMC2679192.
- 862 92. Cheng CY, Reich D, Coresh J, Boerwinkle E, Patterson N, Li M, et al. Admixture mapping of
863 obesity-related traits in African Americans: the Atherosclerosis Risk in Communities (ARIC) Study.
864 *Obesity* (Silver Spring). 2010;18(3):563-72. Epub 2009/08/22. doi: 10.1038/oby.2009.282. PubMed
865 PMID: 19696751; PubMed Central PMCID: PMC2866099.
- 866 93. Torgerson DG, Gignoux CR, Galanter JM, Drake KA, Roth LA, Eng C, et al. Case-control
867 admixture mapping in Latino populations enriches for known asthma-associated genes. *Journal of*
868 *Allergy and Clinical Immunology*. 2012;130(1):76-82. e12.
- 869 94. Shriner D. Overview of admixture mapping. *Curr Protoc Hum Genet*. 2013;Chapter 1:Unit 1 23.
870 Epub 2013/01/15. doi: 10.1002/0471142905.hg0123s76. PubMed PMID: 23315925; PubMed Central
871 PMCID: PMC3556814.
- 872 95. Galanter JM, Gignoux CR, Torgerson DG, Roth LA, Eng C, Oh SS, et al. Genome-wide association
873 study and admixture mapping identify different asthma-associated loci in Latinos: the Genes-
874 environments & Admixture in Latino Americans study. *J Allergy Clin Immunol*. 2014;134(2):295-305.
875 Epub 2014/01/11. doi: 10.1016/j.jaci.2013.08.055. PubMed PMID: 24406073; PubMed Central
876 PMCID: PMC4085159.
- 877 96. Spear ML, Hu D, Pino-Yanes M, Huntsman S, Eng C, Levin AM, et al. A Genome-wide Association
878 and Admixture Mapping Study of Bronchodilator Drug Response in African Americans with Asthma.
879 *bioRxiv*. 2017. doi: 10.1101/157198.
- 880 97. Mak AC, White MJ, Eckalbar WL, Szpiech ZA, Oh SS, Pino-Yanes M, et al. Whole Genome
881 Sequencing of Pharmacogenetic Drug Response in Racially Diverse Children with Asthma. *Am J Respir*

- 882 Crit Care Med. 2018. Epub 2018/03/07. doi: 10.1164/rccm.201712-2529OC. PubMed PMID:
883 29509491.
- 884 98. Lohmueller KE, Indap AR, Schmidt S, Boyko AR, Hernandez RD, Hubisz MJ, et al. Proportionally
885 more deleterious genetic variation in European than in African populations. *Nature*.
886 2008;451(7181):994-7. Epub 2008/02/22. doi: 10.1038/nature06611. PubMed PMID: 18288194;
887 PubMed Central PMCID: PMCPMC2923434.
- 888 99. Tennessen JA, Bigham AW, O'Connor TD, Fu W, Kenny EE, Gravel S, et al. Evolution and
889 functional impact of rare coding variation from deep sequencing of human exomes. *Science*.
890 2012;337(6090):64-9. Epub 2012/05/19. doi: 10.1126/science.1219240. PubMed PMID: 22604720;
891 PubMed Central PMCID: PMCPMC3708544.
- 892 100. Fu W, O'Connor TD, Jun G, Kang HM, Abecasis G, Leal SM, et al. Analysis of 6,515 exomes
893 reveals the recent origin of most human protein-coding variants. *Nature*. 2013;493(7431):216-20.
894 Epub 2012/12/04. doi: 10.1038/nature11690. PubMed PMID: 23201682; PubMed Central PMCID:
895 PMCPMC3676746.
- 896 101. Henn BM, Botigue LR, Bustamante CD, Clark AG, Gravel S. Estimating the mutation load in
897 human genomes. *Nat Rev Genet*. 2015;16(6):333-43. Epub 2015/05/13. doi: 10.1038/nrg3931.
898 PubMed PMID: 25963372; PubMed Central PMCID: PMCPMC4959039.
- 899 102. Szpiech ZA, Blant A, Pemberton TJ. GARLIC: Genomic Autozygosity Regions Likelihood-based
900 Inference and Classification. *Bioinformatics*. 2017;33(13):2059-62. Epub 2017/02/17. doi:
901 10.1093/bioinformatics/btx102. PubMed PMID: 28205676; PubMed Central PMCID:
902 PMCPMC5870576.
- 903 103. Adzhubei IA, Schmidt S, Peshkin L, Ramensky VE, Gerasimova A, Bork P, et al. A method and
904 server for predicting damaging missense mutations. *Nat Methods*. 2010;7(4):248-9. Epub
905 2010/04/01. doi: 10.1038/nmeth0410-248. PubMed PMID: 20354512; PubMed Central PMCID:
906 PMCPMC2855889.
- 907 104. Ng PC, Henikoff S. SIFT: Predicting amino acid changes that affect protein function. *Nucleic
908 Acids Res*. 2003;31(13):3812-4. Epub 2003/06/26. PubMed PMID: 12824425; PubMed Central
909 PMCID: PMCPMC168916.
- 910 105. Kumar P, Henikoff S, Ng PC. Predicting the effects of coding non-synonymous variants on
911 protein function using the SIFT algorithm. *Nat Protoc*. 2009;4(7):1073-81. Epub 2009/06/30. doi:
912 10.1038/nprot.2009.86. PubMed PMID: 19561590.
- 913 106. Choi Y, Chan AP. PROVEAN web server: a tool to predict the functional effect of amino acid
914 substitutions and indels. *Bioinformatics*. 2015;31(16):2745-7. Epub 2015/04/09. doi:
915 10.1093/bioinformatics/btv195. PubMed PMID: 25851949; PubMed Central PMCID:
916 PMCPMC4528627.
- 917 107. Cooper GM, Stone EA, Asimenos G, Program NCS, Green ED, Batzoglou S, et al. Distribution and
918 intensity of constraint in mammalian genomic sequence. *Genome Res*. 2005;15(7):901-13. Epub
919 2005/06/21. doi: 10.1101/gr.3577405. PubMed PMID: 15965027; PubMed Central PMCID:
920 PMCPMC1172034.
- 921 108. Genomes Project C, Auton A, Brooks LD, Durbin RM, Garrison EP, Kang HM, et al. A global
922 reference for human genetic variation. *Nature*. 2015;526(7571):68-74. Epub 2015/10/04. doi:
923 10.1038/nature15393. PubMed PMID: 26432245; PubMed Central PMCID: PMCPMC4750478.
- 924 109. Kircher M, Witten DM, Jain P, O'Roak BJ, Cooper GM, Shendure J. A general framework for
925 estimating the relative pathogenicity of human genetic variants. *Nat Genet*. 2014;46(3):310-5. Epub
926 2014/02/04. doi: 10.1038/ng.2892. PubMed PMID: 24487276; PubMed Central PMCID:
927 PMCPMC3992975.
- 928 110. Lohmueller KE. The distribution of deleterious genetic variation in human populations. *Curr
929 Opin Genet Dev*. 2014;29:139-46. Epub 2014/12/03. doi: 10.1016/j.gde.2014.09.005. PubMed PMID:
930 25461617.

- 931 111. Pedersen CT, Lohmueller KE, Grarup N, Bjerregaard P, Hansen T, Siegismund HR, et al. The
932 Effect of an Extreme and Prolonged Population Bottleneck on Patterns of Deleterious Variation:
933 Insights from the Greenlandic Inuit. *Genetics*. 2017;205(2):787-801. Epub 2016/12/03. doi:
934 10.1534/genetics.116.193821. PubMed PMID: 27903613; PubMed Central PMCID: PMC5289852.
- 935 112. Mezzavilla M, Vozzi D, Badii R, Alkowari MK, Abdulhadi K, Girotto G, et al. Increased rate of
936 deleterious variants in long runs of homozygosity of an inbred population from Qatar. *Hum Hered*.
937 2015;79(1):14-9. Epub 2015/02/28. doi: 10.1159/000371387. PubMed PMID: 25720536.
- 938 113. Mooney J, Huber C, Service S, Sul JH, Marsden C, Zhang Z, et al. Understanding the Hidden
939 Complexity of Latin American Population Isolates. *bioRxiv*. 2018. doi: 10.1101/340158.
- 940 114. Pino-Yanes M, Thakur N, Gignoux CR, Galanter JM, Roth LA, Eng C, et al. Genetic ancestry
941 influences asthma susceptibility and lung function among Latinos. *J Allergy Clin Immunol*.
942 2015;135(1):228-35. Epub 2014/10/11. doi: 10.1016/j.jaci.2014.07.053. PubMed PMID: 25301036;
943 PubMed Central PMCID: PMC4289103.
- 944 115. Drake KA, Torgerson DG, Gignoux CR, Galanter JM, Roth LA, Huntsman S, et al. A genome-wide
945 association study of bronchodilator response in Latinos implicates rare variants. *J Allergy Clin*
946 *Immunol*. 2014;133(2):370-8. Epub 2013/09/03. doi: 10.1016/j.jaci.2013.06.043. PubMed PMID:
947 23992748; PubMed Central PMCID: PMC3938989.
- 948 116. Delaneau O, Zagury JF, Marchini J. Improved whole-chromosome phasing for disease and
949 population genetic studies. *Nat Methods*. 2013;10(1):5-6. Epub 2012/12/28. doi:
950 10.1038/nmeth.2307. PubMed PMID: 23269371.
- 951 117. Maples BK, Gravel S, Kenny EE, Bustamante CD. RFMix: a discriminative modeling approach for
952 rapid and robust local-ancestry inference. *Am J Hum Genet*. 2013;93(2):278-88. Epub 2013/08/06.
953 doi: 10.1016/j.ajhg.2013.06.020. PubMed PMID: 23910464; PubMed Central PMCID:
954 PMC3738819.
- 955 118. Liu X, White S, Peng B, Johnson AD, Brody JA, Li AH, et al. WGS: an annotation pipeline for
956 human genome sequencing studies. *J Med Genet*. 2016;53(2):111-2. Epub 2015/09/24. doi:
957 10.1136/jmedgenet-2015-103423. PubMed PMID: 26395054; PubMed Central PMCID:
958 PMC5124490.
959